

Modeling and Analysis of Hormone and Mitogenic Signal Integration in Prostate Cancer

Katharine V. Rogers, Joseph A. Wayman, Ryan Tasseff, Timothy Chu, Kyriakos Tsahalis, Spencer Davis, Rohit Yallamraju, Gongcheng Lu, Matthew P. DeLisa, and Jeffrey D. Varner*

School of Chemical and Biomolecular Engineering
Cornell University, Ithaca NY 14853

Running Title: Modeling signal transduction in prostate cancer

To be submitted: *Molecular Systems Biology*

*Corresponding author:

Jeffrey D. Varner,

Associate Professor, School of Chemical and Biomolecular Engineering,
244 Olin Hall, Cornell University, Ithaca NY, 14853

Email: jdv27@cornell.edu

Phone: (607) 255 - 4258

Fax: (607) 255 - 9166

Abstract

Prostate cancer is the most common cancer in men and the second leading cause of cancer related death in the United States. Androgens, such as testosterone, are required for prostate cancer growth. Androgen ablation in combination with radiation or chemotherapy remains the primary non-surgical treatment for androgen dependent prostate cancer. However, androgen ablation typically fails to permanently arrest cancer progression, often resulting in castration resistant prostate cancer (CRPC). CRPC is closely related to metastasis and decreased survival. In this study, we developed and analyzed a population of mathematical models describing growth factor and hormone signal integration in androgen dependent, intermediate and resistant prostate cancer cells. The model describes the integration of two simultaneous extracellular signaling inputs, namely, androgen and growth factors into a G1/S cell cycle checkpoint decision. Model parameters were identified from 43 studies in androgen dependent and resistant LNCaP cell lines. The model was validated by comparing simulations with an additional 29 data sets from LNCaP cell lines that were not used during training. Additionally, data from four drug trials was also used to evaluate the model's performance. Sensitivity analysis, conducted over an ensemble of prostate signaling models, suggested that in an androgen free environment general translation and transcription was more sensitive in androgen dependent cells, while in androgen independent cells the PI3K and MAPK pathway species were more sensitive. In a constant DHT environment sensitive species were conserved between the cell lines. These results suggest targeting the PI3K and MAPK pathways in addition to anti-androgen therapies as a treatment for AIPC.

Keywords: Prostate cancer, signal transduction, mathematical modeling

1 Introduction

2 Prostate cancer (PCa) is the most commonly diagnosed cancer and the second leading
3 cause of cancer-related death in men in the United States [80]. Initially, PCa cells depend
4 upon the activation of cytosolic androgen receptors (AR) by androgen hormones, such
5 as testosterone, for survival and growth. Androgen ablation in combination with radiation
6 or chemotherapy remains the primary non-surgical treatment for androgen dependent
7 prostate cancer (ADPC) [41]. However, androgen ablation typically fails to permanently
8 arrest cancer progression as malfunctioning cells eventually lose androgen sensitivity and
9 proliferate without hormone. The loss of androgen sensitivity results in castration resistant
10 prostate cancer (CRPC), a phenotype closely linked with metastasis and greatly reduced
11 survival [33]. Currently, there are six approved treatments that demonstrate a survival
12 advantage in patients with metastatic CRPC, each of these target diverse aspects of the
13 disease [74]. The taxane family members docetaxel and cabazitaxel interact with micro-
14 tubule stability [18, 88], while abiraterone [74] or enzalutamide [76] interfere with androgen
15 signaling by blocking androgen formation or nuclear translocation, respectively. Other ap-
16 proved treatments are non-specific to PCa. For example, general treatments such as
17 sipuleucel-T, a first generation cancer vaccine [43], and radium-223, an alpha emitter
18 which targets bone metastasis [66], are both approved to treat CRPC. Unfortunately, re-
19 gardless of the therapeutic approach, the survival advantage of these treatments is typi-
20 cally only a few months. Thus, understanding the molecular basis of the loss of androgen
21 sensitivity in CRPC could be an important step for the development of the next generation
22 of therapies with a prolonged survival advantage.

23 Androgen-induced proliferation and survival depends upon many coordinated signal
24 transduction and gene expression events. Androgen Receptor (AR) is part of the nu-
25 clear hormone receptor superfamily, which includes other important cancer targets such
26 as progesterone receptor (PR) and estrogen receptor (ER) in breast cancer [2]. Nuclear

27 hormone receptors act as ligand dependent transcription factors interacting with specific
28 DNA sequences of target genes as either monomers, heterodimers, or homodimers; AR,
29 PR, and ER act as homodimers. In the case of AR these specific DNA sequences are
30 known as androgen response elements (ARE) [59]. In the absence of androgen, AR
31 is predominately found in the cytoplasm bound to heat shock proteins (HSP) [72]. An-
32 drogen, either testosterone or testosterone metabolites such as 5α -dihydrotestosterone
33 (DHT), enter prostate cells and interact with the cytosolic androgen receptor (AR). The in-
34 teraction of DHT with AR promotes the dissociation of AR from chaperones such as HSP
35 [71] and its subsequent dimerization, phosphorylation and translocation to the nucleus
36 (reviewed by Brinkmann *et al.* [4]). Activated nuclear AR drives a gene expression pro-
37 gram broadly referred to as androgen action, that promotes both proliferation and survival.
38 In addition to many genes including itself, activated nuclear AR promotes the expression
39 and secretion of prostate specific antigen (PSA), arguably the best known PCa biomarker
40 [21]. PSA is commonly used as a prostate cancer indicator, although its prognostic ability
41 is controversial [3, 39, 63]. In CRPC, AR signals in the absence of androgens. Andro-
42 gen dependent (AD) prostate cells can become castration resistant (CR) through several
43 possible mechanisms, including constitutively amplified AR expression and altered AR
44 sensitivity to testosterone or other non-androgenic molecules [21]. In this study, we fo-
45 cused on the aberrant activation of AR by kinase signaling cascades, sometimes called
46 the outlaw pathway. Outlaw pathway activation is driven by over-activated receptor tyro-
47 sine kinases (RTKs), a common pathology in many cancer types including PCa [15, 81].
48 RTKs stimulate downstream kinases, including the AKT and mitogen-activated protein
49 kinase (MAPK) pathways, which promote AR phosphorylation and dimerization in the ab-
50 sence of an androgen signal [15, 101]. Interestingly, among the few genes activated AR
51 represses is cellular prostatic acid phosphatase (cPAcP), itself a key regulatory of RTK ac-
52 tivation [92]. Thus, in CRPC the androgen program is initiated without the corresponding

53 extracellular hormone cue, potentially from crosstalk between growth factor and hormone
54 receptor pathways.

55 In this study, we developed a mathematical model of growth factor and hormone signal
56 integration in androgen dependent, intermediate and resistant prostate cancer cells. We
57 used this model to better understand which components and processes were differentially
58 important in AD versus CR cells. The new model architecture was a significant advance
59 over our previous prostate signaling model [89]. We added the regulated expression of ten
60 additional proteins, including the cell cycle restriction point proteins cyclin D (and the dif-
61 ferentially spliced variants cyclin D1a and cyclin D1b), cyclin E, cyclin-dependent kinase
62 inhibitor 1A (p21Cip1), and cyclin-dependent kinase inhibitor 1B (p27Kip1). Also, we in-
63 cluded the Rb/E2F pathway, expanded our description of the activation of the mammalian
64 target of rapamycin (mTOR) protein and its role in translation initiation, and included the
65 regulation of AR action by cyclin D1a and E2F. However, this upgraded architecture, while
66 increasing the biological scope of the model, also expanded the number of unknown
67 model parameters. To estimate these parameters, we used multiobjective optimization
68 in combination with dynamic and steady-state data sets generated in AD, intermediate
69 and CR LNCaP cell lines. We identified a population of approximately $N = 5000$ models
70 (from well over a million candidate models) which described both AD and CR data sets
71 using a single model structure. Furthermore, we tested the model using an additional 29
72 LNCaP data sets not used for model training, along with four drug studies. We analyzed
73 the model population using sensitivity and robustness analysis to uncover differentially
74 important mechanisms in AD versus CR cell lines. In the presence of androgen, the sen-
75 sitivity profile was similar between AD and CR cells. Components of the MAPK and PI3K
76 pathways were highly fragile, irrespective of the level of androgen dependence. However,
77 in the absence of androgen, there were 609 statistically significant shifts in species sen-
78 sitivity between AD and CR cells. Of these, 108 were larger than one standard deviation

79 above the mean. In CR cells, HER2 activation of the MAPK and PI3K pathways was
80 significantly more important, as was AR activation through the MAPK pathway. On the
81 other hand, components of the translation and transcription infrastructure were differen-
82 tially more important in AD cells in the absence of androgen. Taken together, our analysis
83 suggested that independently targeting the PI3K or MAPK pathways in combination with
84 anti-androgen therapies could perhaps be an effective treatment strategy for CRPC.

85 **Results**

86 **Estimating an ensemble of prostate signaling models.** We modeled the integration
87 of growth factor, cell cycle and hormone signaling pathways in AD and CR LNCaP cells
88 (Fig. 1). The signaling architecture was hand curated from over 80 primary literature
89 sources in combination with biological databases. The model equations were formulated
90 as a system of ordinary differential equations (ODEs), where biochemical reaction rates
91 were modeled using mass action kinetics. ODEs and mass action kinetics are common
92 modeling tools [94], however, ODEs have the disadvantage of requiring estimates for
93 unknown model parameters. Many techniques have been developed to estimate ODE
94 model parameters, often from noisy and sparse experimental data [62]. Typically these
95 identification problems are underdetermined, hence no unique parameter values can be
96 estimated [93]. Thus, instead of estimating a single yet highly uncertain parameter set, we
97 estimated an ensemble of possible parameter sets using the Pareto Optimal Ensemble
98 Techniques (POETs) algorithm [83]. POETs uses a combination of simulated annealing
99 and local optimization techniques coupled with Pareto optimality-based ranking to simul-
100 taneously optimize multiple objective functions. Starting from an initial best fit set, we
101 estimated the 1687 unknown model parameters (1674 kinetic parameters and 13 non-
102 zero initial conditions) using 43 *in vitro* data sets taken from AD, intermediate and CR
103 LNCaP cells (Table T1). Each of the 43 training data sets was a separate objective in the
104 multiobjective calculation. The training data were steady-state or dynamic immunoblots
105 from which we extracted relative species abundance from their optical density profiles.
106 POETs sampled well over a million possible parameter sets, from which we selected N
107 = 5000 sets for further analysis. Over the ensemble, the coefficient of variation (CV) of
108 the kinetic parameters spanned 0.5 - 5.8, with 33% of the parameters having a CV of
109 less than one (Fig. ZZ). As a control, we also performed simulations for R = 100 random
110 parameter sets to compare against the ensemble generated by POETs.

The ensemble of PCa models recapitulated training data in both AD and CR cell lines with only two experimentally justified parameter changes (Fig. 2 and Fig. 3). Data from the LNCaP clones C-33 (dependent), C-51 (intermediate), and C-81 (resistant) [40, 42, 53] along with the CR LNCaP cell lines LNCaP-Rf [64], LNCaP-AI [10] and LNAI [25] were used for model identification. To simulate the effective difference between LNCaP cell lines, the parameter controlling the maximum rate of PAcP gene expression was scaled by 0.1 and 0.5, respectively, for the C-81 and C-51 cell-lines compared to C-33. This modification was based upon steady-state PAcP data from the three LNCaP clones [48]. Similarly, the expression of p16INK4 was adjusted in accordance with the study of Lu *et al.* [58]. These two parameters were the only adjustable parameter differences between AD and CR cells. To simulate an increased mTOR activation in the presence of a DHT stimulus, we added a first order activation term for mTOR activation with a DHT stimulus. Androgens have been shown to increase expression of proteins involved in cellular metabolism, which may lead to an increase in mTOR activation [99]. The model fit 36 of the 43 training objectives for greater than 40% of the ensemble members (Fig. 2A). Conversely, only 10 of the 43 training objectives were captured with the random parameter control (Fig. 2B). The model captured the crosstalk between RTK activation and androgen action (Fig. 3). The model described DHT-induced PSA expression in both C-33 (Fig. 3A) and C-81 (Fig. 3B) cells. Interestingly, simulations with the HER2 inhibitor AG879 recapitulated decreased PSA expression in C-81 cells (Fig. 3C) in the absence of androgen stimulation. AR action decreased the PAcP mRNA message (Fig. 3D), presumably leading to increased HER2 activity. The model also recapitulated the integration of androgen action with AR expression, G1/S cell cycle protein expression and AKT phosphorylation. For example, the model captured AR-induced AR expression following a DHT stimulus (Fig. 3H). Conversely, the transcription factor E2F inhibits AR transcription in LNCaP cells (Fig. 3I). Other cell cycle proteins were also integrated with

137 androgen action. For example, the cyclin D1 abundance increased in CR compared to
138 AD cells in the absence of androgen (Fig. 3E), while DHT induced p21Cip1 expression
139 in C-33 cells (Fig. 3F). The level of phosphorylated AKT was also increased in higher
140 passage number cells (Fig. 3G). Taken together, [FINISH ME].

141 **Validation simulations revealed missing network structure.** The model was vali-
142 dated against 29 *in vitro* and four *in vivo* studies (Table T2). For 15 of the 29 cases,
143 greater than 40% of the ensemble was qualitatively consistent with the experimental data
144 (Fig. 2C). However, for the random parameter control, only 7 of the 29 cases were sat-
145 isfied (Fig. 2D). We correctly predicted positive feedback between HER2 auto-activation
146 and androgen action (Fig. 4A and Fig. 4B). We also captured the dose-dependence of
147 AR abundance on DHT (Fig. 4C). In addition to the cell line studies, we simulated the
148 outcome of enzalutamide, lapatinib, and sorafenib clinical trials in AD and CRPC patients.
149 The trial end points were the reduction in PSA expression relative to an untreated base-
150 line. Enzalutamide acts on AR by inhibiting its nuclear translocation, DNA binding, and
151 coactivator recruitment [76]. In the enzalutamide trial, 54% of the patients that received
152 the drug showed a PSA decline of $\geq 50\%$ while 25% showed a decline $\geq 90\%$. We
153 simulated enzalutamide exposure by reducing the rate constants governing activated AR
154 binding to nuclear importer, cyclin E, and CDK6 to 1% of their initial values. Consistent
155 with the trial, 62% of ensemble members showed a $\geq 50\%$ decline in PSA abundance,
156 while 14% showed a $\geq 90\%$ decline (Fig. 4G). The second trial we simulated involved ex-
157 posure of CRPC patients to sorafenib. Sorafenib is a kinase inhibitor with activity against
158 Raf, vascular endothelial growth factor receptor (VEGFR), platelet-derived growth factor
159 receptor (PDGFR), c-kit and c-Ret [16]. We considered only the effects of sorafenib on the
160 protein kinase Raf, as VEGFR, PDGFR, c-kit and c-Ret were not included in the model.
161 None of the 22 patients in the sorafenib study showed a PSA decline of $> 50\%$. However,
162 our simulations showed that approximately 55% of the ensemble members had a PSA

163 decline of $\geq 50\%$. The last drug we considered was lapatinib, an inhibitor of epidermal
164 growth factor receptor (EGFR) and HER2 tyrosine kinase activity [56]. Two lapatinib drug
165 trials were considered: one in which patients had CRPC and one in which patients had
166 biochemically relapsed ADPC [56, 97]. In the CRPC lapatinib drug trial, two of the 21 en-
167 rolled patients had a PSA response $\geq 47\%$ [97]. For the CRPC case, our model showed
168 26.5% of ensemble members with a PSA response $\geq 47\%$. Of the 35 patients enrolled in
169 the ADPC lapatinib study, no PSA decreases was observed [56]. In this case, our model
170 showed 9.2% of ensemble members with a PSA response $\geq 50\%$. Although no response
171 to lapatinib was seen in ADPC clinical trials, *in vitro* AD LNCaP experiments showed de-
172 creased PSA expression in response to lapatinib, most notably with the addition of DHT
173 [57].

174 Validation and training failures suggested the original signaling architecture was miss-
175 ing critical components. Several of the failed training and validation simulations involved
176 the response of the network to epidermal growth factor (EGF) stimulation. For example,
177 Chen *et al.* showed that HER2 phosphorylation increased within five minutes following
178 EGF stimulation of LNCaP-AI cells [10]. We predicted no connection between HER2
179 phosphorylation and EGF stimulation on this short timescale (Fig. 4E). Interestingly, we
180 initially neglected the heterodimerization of HER2 with other ErbB family members in or-
181 der to simplify the model. However, Chen *et al.* suggested that HER2-EGFR heterodimer-
182 ization could be an important factor in EGF-driven activation of HER2 [10]. We tested this
183 hypothesis by developing a new model that included HER2 and EGFR heterodimeriza-
184 tion. We set the rate constants governing the assembly of HER2/EGFR heterodimers
185 equal to EGFR homodimer assembly; all other parameters were unchanged. This was
186 a reasonable first approximation, as the affinity of HER2/EGFR heterodimerization and
187 EGFR homodimerization is thought to be similar [37]. With the inclusion of HER2-EGFR
188 heterodimerization, we qualitatively fit the EGF-induced HER2 activation case and im-

189 proved our training for experiments that involved an EGF stimulus, e.g., cyclin D mRNA
190 and protein abundance following an EGF stimulus in C-33 cells (Fig 2A and C, white
191 pixels).

192 **Sensitivity analysis identified differentially important features of the prostate ar-**
193 **chitecture.** We used sensitivity analysis to identify important signaling components in
194 AD versus CR cells (Fig. 5). We calculated first order steady-state sensitivity coefficients
195 under different stimuli for 500 parameter sets selected from the ensemble. Signaling com-
196 ponents were rank-ordered based upon analysis of their sensitivity coefficient values. In
197 the presence of DHT, the sensitivity profile was similar for AD versus CR cells, with only a
198 few differences (Fig. 5B). The top 2% of sensitive species, regardless of androgen depen-
199 dence, involved components from the MAPK and PI3K pathways. In particular, activated
200 Ras, Raf, phosphorylated MEK, as well as PIP3 localized AKT, phosphorylated AKT, and
201 PI3K were sensitive in both AD and CR cells. Species involving PAcP and p16INK4 were
202 more sensitive in AD cells, which was expected since the expression of these two proteins
203 were the only parameters changed between AD and CR cells. Other species such as E2F,
204 cyclin E, and DHT-activated AR were also more sensitive in AD cells. On the other hand,
205 HER2-Grb2-Gab activation of PI3K and AKT inhibition of RAF were more sensitive in CR
206 cells.

207 The importance of signaling components varied with androgen dependence in the ab-
208 sence of DHT (Fig. 5A). There were 609 statistically significant shifts in species sensitivity
209 (318 more and 291 less sensitive) between CR and AD cells in a non-androgen environ-
210 ment. However, only 108 of these shifts were greater than one standard deviation above
211 the mean. In CR cells, HER2 activation of ERK and PI3K was more sensitive, as was AR
212 activation through the MAPK pathway. This was expected, as outlaw pathway activity was
213 elevated in castration resistant cells. Species in the MAPK pathway were in general more
214 sensitive in CR cells (128 out of 140 significant), with all forms of sPAcP more robust in

215 CR cells. On the other hand, infrastructure pathways encoding transcription and transla-
216 tion were more sensitive in AD cells. PSA and cyclin D1b (mRNA and mRNA complexes)
217 were the only species involved in translation that were more robust in AD cells (14 out of
218 116). The transcription factor, E2F was more fragile in AD cells, while the transcription
219 factors ETS and AP1 were more robust. ETS and AP1 are activated by phosphorylated
220 ERK, and ETS is also activated by active PKC [55, 98]. E2F is deactivated through bind-
221 ing to Rb, which is deactivated by cyclin D1 and CDK phosphorylation [46]. The model
222 also included AP1 suppression of AR transcriptional activity (more sensitive in CR) [75],
223 as well as inhibition of transcription of the AR gene by E2F (more sensitive in AD) [17].
224 Species in the PI3K pathway that were more fragile in AD cells included Rheb and TOR
225 complexes. Interestingly, these species were included as the last step in the PI3K path-
226 way prior to translation, with the phosphorylation of 4E-BP1 by TOR being considered the
227 beginning of translation in this model. This again indicates that in the absence of DHT
228 general translation is more fragile in AD cells.

229 There was a large shift in sensitive species between an androgen and a non-androgen
230 environment in both AD and CR cell lines (Fig. 5C and Fig. S1). Of the 664 statis-
231 tically significant shifts in AD cells, 288 were more sensitive between androgen versus
232 non-androgen environments. However, only 119 shifts were larger than one standard
233 deviation above the mean. Unsurprisingly, AR activation through DHT binding, with and
234 without coactivators, in a DHT environment was more sensitive, as was AR inhibition of
235 PAcP transcription (repressed by AR in the model). Species further upstream, such as
236 HER2 activation of the MAPK and PI3K/AKT pathways, were also more sensitive in a DHT
237 environment. Cell cycle species that were more fragile in the presence of DHT, included
238 complexes involving p21Cip1 and CDC25A. In a non-androgen environment, basal tran-
239 scription (68 out of 72) and translation (114 out of 120) were more fragile. Other fragile
240 species in the absence of DHT included Rb, E2F, Sam68, cyclin D1a complexes, phos-

241 phatases in the MAPK pathway, Rheb complexes, and TOR complexes.

242 We also considered the sensitivity of CR cells following the application of the AR in-
243 hibitor enzalutamide in the presence of DHT (Fig. 5D). In an androgen environment
244 with enzalutamide, species which were more fragile included cytosolic AR, cPAcP, and
245 p21Cip1. As we would expect, AR species found in the nucleus and/or bound to coactiva-
246 tors, were more robust in the absence of enzalutamide. The top two percent of sensitive
247 species with and without enzalutamide were conserved. In a CR cell, enzalutamide had
248 no effect on the sensitivity of PI3K/AKT species as well as many MAPK species (ERK,
249 Raf, and MEK). Next, we looked at the effect of enzalutamide on a CR cell in both a non-
250 androgen and DHT environment (Fig. S1). More sensitive species in a non-androgen
251 environment included dimerized HER2, ERK, and PAcP. Species which were more ro-
252 bust in the non-androgen environment included, AR activated by DHT, AKT, p70, and
253 AR bound to HSP. The results of our sensitivity analysis indicate that instead of inhibiting
254 solely the AR pathway (enzalutamide), a combination therapy targeting the PI3K or MAPK
255 pathways in addition to AR may be more effective.

256 **Robustness analysis identified key regulators of prostate cancer.** Robustness anal-
257 ysis was conducted for 80 proteins to quantify the effects of amplifying or knocking down
258 key model components in both AD and CR cells. Gene expression parameters were al-
259 tered by a factor 10, 0.5, and 0 for knock-in, knock-down, or knock-out perturbations,
260 respectively. We calculated the effect of these perturbations on different protein markers,
261 such as PSA, AR, and cyclin D. The results of the model suggest that an inhibition of
262 either the PI3K pathway or the MAPK pathway in combination with an AR inhibitor as a
263 possible therapy for CRPC. Sensitivity analysis revealed no change in the top sensitive
264 species in the presence or absence of the AR inhibitor, enzalutamide. PI3K/AKT and
265 MAPK species continued to fall in the top two percent of sensitive species. A study by
266 Carver *et al.* looked at dual inhibition of AR and PI3K signaling in LNCaP cells and in a

267 Pten-deficient murine prostate cancer model [66]. Using both the PI3K inhibitor, BEZ235,
268 and the AR inhibitor, MDV3100 (enzalutamide), the group saw a drastic decrease in the
269 total number of cells. Each inhibitor on it's own had a much smaller effect on total cell
270 number. They saw an increase in the cell death marker, c-PARP, in the dual inhibition
271 case. The group hypothesized that AKT inhibition leads to increased AR signaling activ-
272 ity through increased protein concentrations of HER3. On the other hand, AR inhibition
273 leads to increased AKT activity due to the down regulation of PHLPP, a protein phos-
274 phatase that regulates AKT. For simplicity, the HER3 pathway and also cell death were
275 not included in the model. Dual knock-out studies of PI3K and AR in our model show no
276 additive effect on any cell cycle proteins through the dual knock-out. The pathways in our
277 model appear to be uncoupled and therefore no synergy is shown in the dual knock-out
278 case. This could indicate that the combined decrease in cell population is entirely due to
279 cell death. The Carver *et al.* study did not consider cell cycle proteins or cell growth. Our
280 model does show a decrease in cell cycle proteins in the PI3K knock-out as well as in the
281 dual knock-out case. This result seems to be consistent with the decreased cell growth
282 in the PI3K knock-out case which is not dependent on cell death, as c-PARP levels are
283 low. The decrease in cell cycle proteins is due to a decrease in general translation, in-
284 cluding free eIF4E levels and activated 40S ribosome subunit. The decrease in p70 (S6)
285 activation due to inhibition of PI3K is shown in both the model and in the Carver *et al.*
286 study (Supplementary Figure), indicating this result is due to the PI3K pathway. It would
287 be interesting to repeat the experiment looking at cell cycle proteins and also performing
288 the experiment in CR LNCaP cells, instead of AD cells.

289 A knock-out of Raf, MEK or ERK showed an overall increase in cyclin D levels in CR
290 cells (Fig. S2). This was unexpected and we saw a similar increase in cyclin D due to
291 the knock-in of Raf, MEK or ERK. We found that individual ensemble members showed
292 different response to a Raf knock-out, in both cyclin D concentration and PSA concentra-

tion. Of the 500 ensemble members, 126 members saw an increase in PSA concentration and 62 members saw an increase in cyclin D concentration due to the knock-out of Raf (Fig. 6). We saw three distinct regions: (1) increase in PSA concentration, (2) increase in cyclin D concentration, and (3) a decrease in both PSA and cyclin D. We explored the flux vectors of the outlying parameter sets to understand the mechanistic effect of Raf knock-out on PSA and cyclin D. Outlying parameter sets in region 1 displayed high activation of PI3K through HER2 signaling as well as high association of AP1 with AR. AP1 binds and suppresses AR transcriptional activity in LNCaP cells [75]. Knocking out Raf lowered AP1 levels and, therefore, freed AR for increased transcription of PSA. In region 2, parameter sets also had high activation of PI3K through HER2. They also had higher association of E2F with Rb and cyclin D1a with AR. Cyclin D levels in this region increase due to an increase in E2F levels caused by the Raf knock-out. Parameters in region 3 have high association of TOR. Interestingly, the drug sorafenib, a multi-kinase inhibitor that has activity against Raf, showed no measurable PSA decline in prostate cancer patients in clinical trials [16]. The robustness analysis showed that network perturbation can result in unexpected responses due to cell-to-cell heterogeneity in gene expression. These outlying cell types could be critical for understanding when designing drug targets and combination therapies.

311 Discussion

312 In this study, we developed a population of mathematical models describing growth fac-
313 tor and hormone signal integration in androgen dependent, intermediate and resistant
314 prostate cancer cells. These models described the regulation of androgen receptor ex-
315 pression and activation through androgen binding as well as a ligand-independent, MAPK-
316 driven mechanism referred to as the outlaw pathway. An ensemble of model parameters
317 was estimated using 43 steady-state and dynamic data sets taken from androgen depen-

318 dent, intermediate and independent LNCaP cell lines using multiobjective optimization.
319 Further, we tested the predictive power of the model by comparing model predictions
320 against 33 novel data sets (including four *in vivo* drug studies) not used during model
321 training. The model ensemble captured 84% of the training data and 52% of the validation
322 data relative to 23% and 24% for a random control population. Interestingly, during the the
323 initial round of parameter estimation, we identified several potentially missing structural
324 components not present in the original connectivity. One such component, EGF-induced
325 HER2/EGFR heterodimerization, was added to the current generation model. Inclusion of
326 this structural component significantly improved both training and validation performance
327 using the same rate constants as the EGFR-homodimer case (no additional parameter
328 fitting). We then analyzed the population of signaling models, using both sensitivity and
329 robustness analysis, to identify the critical components controlling network performance
330 in a variety of conditions.

331 In addition, three of the validation cases involved the effect of EGF on AR and AR-
332 activated genes, i.e., PSA. Cai *et al.* showed decreased expression of endogenous AR
333 as well as androgen-regulated PSA in AD LNCaP cells due to an EGF stimulus [8]. Cinar
334 *et al.* also showed decreased AR protein expression due to EGF, an effect reversed by
335 the mTOR inhibitor, Rapamycin [14]. Model simulations show either the opposite trend
336 or no effect due to EGF stimulus (Fig. 4F) [14]. These results suggest missing network
337 structure. From additional literature searches, the inhibition of AR activation through EGF
338 is still an open question, with many groups debating the biology involved, predominately
339 in the PI3K/AKT pathway. Lin *et al.* found that in low passage number LNCaP cells (C-
340 33), AKT negatively regulates AR by destabilizing it and marking it for ubiquitylation. In
341 high passage number LNCaP (C-81), AKT levels are high which contribute to AR stability
342 and less degradation [51]. Wen *et al.* showed that HER2 could induce AKT activation and
343 LNCaP cell growth in the presence and absence of androgen [96]. Another study shows

344 AKT phosphorylation of AR at S213 and S790 suppresses AR transactivation and AR-
345 mediated apoptosis of LNCaP [52]. The study from Cai *et al.* showed the reduction in AR
346 was not due to degradation or PI3K/AKT signaling, but instead was due to decreased AR
347 mRNA levels [8]. They found that AR protein levels in CR cells were not affected by EGF.
348 Others though have found that PSA expression, even in C-81 cells, is decreased by EGF
349 [31]. In other prostate cell lines, EGF has been shown to increase AR transactivation
350 [27, 70]. The MAPK pathway, which is downstream of EGFR, may also enhance AR
351 responses to low levels of androgen [29, 95]. Due to the discrepancies in the literature,
352 experiments should be performed before adding additional network connectivity to the
353 model.

354 The population of PCa models was analyzed using sensitivity analysis to identify key
355 signaling components and processes in both AD and CR cells. There was very little dif-
356 ference between sensitive and robust components in AD versus CR cells in the presence
357 of androgen. MAPK and PI3K pathway components were consistently ranked in the top
358 2% of sensitive species in the presence of androgen for both AD and CR cells. On the
359 other hand, cell cycle species, such as cyclin D-CDK4/6 complexes bound to cell cycle
360 inhibitors (p27Kip1, p21Cip1, p16INK4), were consistently robust. However, this profile
361 changed considerably in the absence of androgen. The activation of PI3K and ERK by
362 HER2 dimerization and autophosphorylation was significantly more important in CR ver-
363 sus AD cells. Interestingly, AR activation by ERK was also more sensitive in CR versus AD
364 cells in the absence of androgen. Lastly, although AR-regulated transcriptional processes
365 were equally sensitive between the cell types, general translational and transcriptional
366 components were more robust in CR versus AD cells. This evidence supports the current
367 theory that CR cells will still respond to androgen and, thus, AR is still an active target
368 in therapeutic against CRPC [44]. Supporting the argument that AR can be activated in
369 the absence of androgens by MAPK activation [21]. Advanced prostate cancers often

370 have higher levels of E2F and other transcription factors [17]. Interestingly, E2F was more
371 sensitive in AD cells, while other transcription factors (ETS and AP1) were more robust.
372 The drug enzalutamide had no effect on the top 2% of sensitive species. Species in the
373 PI3K/AKT and MAPK pathways in the presence of enzalutamide were still highly sensi-
374 tive. The application of enzalutamide, increased sensitivity of AR species found outside
375 of the nucleus as well as PAcP species. Robustness analysis indicated diverse effects
376 of Raf knock-out on PSA and cyclin D concentrations. Clinical studies of sorafenib, a
377 multi-kinase inhibitor that has activity against Raf, showed increase PSA levels in pa-
378 tients [16]. Our results indicate that cell-to cell heterogeneity in gene expression can play
379 a significant role in determining cell response. Thus, combination therapies need to be
380 considered even in the case of a Raf knock-out.

381 The results of the model suggest that an inhibition of either the PI3K pathway or the
382 MAPK pathway in combination with an AR inhibitor as a possible therapy for CRPC. Sensi-
383 tivity analysis revealed no change in the top sensitive species in the presence or absence
384 of the AR inhibitor, enzalutamide. PI3K/AKT and MAPK species continued to fall in the
385 top two percent of sensitive species. A study by Carver *et al.* looked at dual inhibition
386 of AR and PI3K signaling in LNCaP cells and in a Pten-deficient murine prostate cancer
387 model [66]. Using both the PI3K inhibitor, BEZ235, and the AR inhibitor, MDV3100 (en-
388 zalutamide), the group saw a drastic decrease in the total number of cells. Each inhibitor
389 on its own had a much smaller effect on total cell number. They saw an increase in the
390 cell death marker, c-PARP, in the dual inhibition case. The group hypothesized that AKT
391 inhibition leads to increased AR signaling activity through increased protein concentra-
392 tions of HER3. On the other hand AR inhibition leads to increased AKT activity due to the
393 down regulation of PHLPP, a protein phosphatase that regulates AKT. For the simplicity of
394 this model, the HER3 pathway and also cell death were not included in the model. Dual
395 knock-out studies of PI3K and AR in our model show no additive effect on any cell cycle

396 proteins through the dual knock-out. The pathways in our model appear to be uncoupled
397 and therefore no synergy is shown in the dual knock-out case. This could indicate that
398 the combined decrease in cell population is entirely due to cell death. The Carver *et al.*
399 study did not consider cell cycle proteins or cell growth. Our model does show a decrease
400 in cell cycle proteins in the PI3K knock-out as well as in the dual knock-out case. This
401 result seems to be consistent with the decreased cell growth in the PI3K knock-out case
402 which is not dependent on cell death, as c-PARP levels are low. The decrease in cell
403 cycle proteins is due to a decrease in general translation, including free eIF4E levels and
404 activated 40S ribosome subunit. The decrease in p70 (S6) activation due to inhibition of
405 PI3K is shown in both the model and in the Carver *et al.* study (Supplementary Figure),
406 indicating this result is due to the PI3K pathway. It would be interesting to repeat the ex-
407 periment looking at cell cycle proteins and also performing the experiment in CR LNCaP
408 cells, instead of AD cells.

409 The PCa signaling architecture was assembled after extensive literature review and
410 hand curation of the biochemical interactions. However, there are a number of areas
411 where model connectivity could be refined, e.g., the regulation of AR phosphorylation. We
412 assumed a single canonical activating AR phosphorylation site (S515), with ERK being
413 the major kinase and PP2A or PP1 being the major phosphatases responsible for regulat-
414 ing this site. MAPK activation following EGF treatment increases AR transcription and cell
415 growth, partially through AR phosphorylation on MAPK consensus site S515 [70]. How-
416 ever, there are at least 13 phosphorylation sites identified on AR, with phosphorylation at
417 six of these being androgen induced [24]. Moreover, other kinases such as AKT, protein
418 kinase C (PKC) family members, as well as Src-family kinases can all phosphorylate AR
419 in prostate cells [29, 70]. For example, AKT activation leads to AR phosphorylation at both
420 S213 and S791 (however, the role of these sites remains unclear) [51, 52, 87, 96]. AKT
421 effects on AR may also be passage number dependent, with AKT repressing AR transcrip-

tion in low passage number cells and enhancing transcription in higher passage numbers [51]. Androgen independent phosphorylation of AR by Src family kinases (not currently in model) at Y534 [29] or by protein kinase C (PKC) family members at the consensus site S578 could also be important for understanding the regulation of AR activity. A second area we will revisit is the gene expression program associated with androgen action, and particularly the role of AR coregulators. Currently, we included only two AR coactivators, cyclin E and CDK6 [50, 100] and three corepressors AP1, Cdc25A, and cyclin D1a in the model [12, 69, 75]. However, there are at least 169 proteins classified as potential AR coregulators [34, 35] with many of these being differentially expressed in malignant cells. For example, the expression of steroid receptor coactivator-1 (Src-1) and transcriptional intermediary factor 2 (Tif-2), both members of the steroid receptor coactivator family, are elevated in prostate cancer [27, 28]. Src-1 is phosphorylated by MAPK and interacts directly with AR to enhance AR-mediated transcription [34]. Another class of potentially important AR coregulators are the cell cycle proteins Cdc25 and Rb. Unlike Cdc25A, Cdc25B (not in the model) can act as an AR coactivator leading to enhanced AR transcription activity [65]. The Rb protein, in addition to being a key cell cycle regulator, has been shown to be an AR coactivator in an androgen-independent manner in DU145 cells [102]. However, there is some uncertainty about the role of Rb as Sharma *et al.* showed that Rb decreased AR activation in multiple prostate cancer cell lines and xenografts [78]. Forkhead proteins have also been shown to activate as well as repress AR function. In prostate cancer, AKT suppresses AFX/Forkhead proteins, which diminishes expression of AFX target genes, such as p27Kip1 [6, 26, 60, 85]. Lastly, undoubtedly there are several other signaling axes important in PCa, such as cytokine or insulin- and insulin-like growth factor signaling [9, 36, 77, 86]. Understanding the pathways associated with these signals and how they relate to the current model, may give us a more complete picture of CR prostate cancer.

448 **Materials and Methods**

449 **Prostate model signaling architecture.** We modeled the expression, translation and
450 post-translational modifications of key components of the signaling architecture. The
451 model, which consisted of 780 protein, lipid or mRNA species interconnected by 1674
452 interactions, was a significant extension to our previous model [89] in several important
453 areas. First, we included well-mixed nuclear, cytosolic, membrane and extracellular com-
454 partments (including transfer terms between compartments). Next, we expanded the
455 description of growth factor receptor signaling, considering both homo- and heterodimer
456 formation between ErbB family members and the role of cellular and secreted prostatic
457 acid phosphatase (cPAcP and sPAcP, respectively). Both forms of PAcP were included
458 because cPAcP downregulates HER2 activity, while sPAcP promotes modest HER2 ac-
459 tivation [92]. Third, we expanded the description of the G1/S transition of the cell cycle
460 (restriction point). The previous model used the abundance of cyclin D as a proliferation
461 marker, but did not include other proteins or interactions potentially important to the re-
462 striction point. Toward this shortcoming, we included cyclin E expression (and its role as
463 a coregulator of androgen receptor expression), enhanced the description of cyclin D ex-
464 pression and the alternative splicing of cyclin D mRNA (including the role of the splice vari-
465 ants in androgen action), included the Rb/E2F pathway as well as E2F inhibition of andro-
466 gen receptor expression [17], and the cyclin-dependent kinases cyclin-dependent kinase
467 4 (CDK4) and cyclin-dependent kinase 6 (CDK6). We also included key inhibitors of the
468 restriction point including cyclin-dependent kinase inhibitor 1 (p21Cip1), cyclin-dependent
469 kinase inhibitor 1B (p27Kip1), and cyclin-dependent kinase inhibitor 2A (p16INK4) [79].
470 Fourth, we enhanced the description of growth factor induced translation initiation. One
471 of the key findings of the previous model was that growth factor induced translation ini-
472 tiation was globally sensitive (important in both androgen dependent and independent
473 conditions). However, the description of this important subsystem was simplified in the

474 previous model. Here, we expanded this subsystem, using connectivity similar to previ-
 475 ous study of Lequieu *et al.* [49], and re-examined the importance of key components of
 476 this axis, such as mammalian target of rapamycin (mTOR), phosphatidylinositide 3-kinase
 477 (PI3K) and AKT. Lastly, we significantly expanded the description of the role of androgen
 478 receptor. The previous model assumed constant AR expression, consistent with studies
 479 in androgen dependent and independent LNCaP sublines [48]. However, other prostate
 480 cancer cell lines vary in their AR expression [82]. Thus, to capture androgen signaling in
 481 a variety of prostate cancer cells, we included the transcriptional regulation governing an-
 482 drogen receptor expression, updated our description of the regulation of androgen recep-
 483 tor activity and androgen action (gene expression program driven by activated androgen
 484 receptor). At the expression level, we included AR auto-regulation in combination with the
 485 co-activators cyclin E and CDK6 [50, 100]. We also assumed androgen receptor could be
 486 activated through androgen binding or a ligand-independent, MAPK-driven mechanism
 487 referred to as the outlaw pathway [21, 101]. We assumed a single canonical activating
 488 AR phosphorylation site (S515), with phosphorylated extracellular-signal-regulated kinase
 489 1/2 (ppERK1/2) being the major kinase and protein phosphatase 2 (PP2A) or phospho-
 490 protein phosphatase 1 (PP1) being the major phosphatases responsible for regulating this
 491 site. Finally, we modeled androgen receptor induced gene expression, including prostate
 492 specific antigen (PSA), cPAcP and p21Cip1.

493 **Formulation and solution of the model equations.** The prostate model was formu-
 494 lated as a coupled set of non-linear ordinary differential equations (ODEs):

$$\frac{dx}{dt} = S \cdot r(x, k) \quad x(t_0) = x_0 \quad (1)$$

495 The quantity x denotes the vector describing the abundance of protein, mRNA, and other
 496 species in the model (780×1). The stoichiometric matrix S encodes the signaling architec-

497 ture considered in the model (780×1674). Each row of \mathbf{S} describes a signaling component
 498 while each column describes a particular interaction. The (i, j) element of \mathbf{S} , denoted by
 499 σ_{ij} , describes how species i is involved with interaction j . If $\sigma_{ij} > 0$, species i is produced
 500 by interaction j . Conversely, if $\sigma_{ij} < 0$, then species i is consumed in interaction j . Lastly,
 501 if $\sigma_{ij} = 0$, then species i is not involved in interaction j . The term $\mathbf{r}(\mathbf{x}, \mathbf{k})$ denotes the vec-
 502 tor of interactions rates (1674×1). Gene expression and translation processes as well as
 503 all biochemical transformations were decomposed into simple elementary steps, where
 504 all reversible interactions were split into two irreversible steps (supplemental materials).
 505 We modeled each network interaction using elementary rate laws where all reversible in-
 506 teractions were split into two irreversible steps. Thus, the rate expression for interaction q
 507 was given by:

$$r_q(\mathbf{x}, k_q) = k_q \prod_{j \in \{\mathbf{R}_q\}} x_j^{-\sigma_{jq}} \quad (2)$$

508 The set $\{\mathbf{R}_q\}$ denotes reactants for reaction q , while σ_{jq} denotes the stoichiometric co-
 509 efficient (element of the matrix \mathbf{S}) governing species j in reaction q . The quantity k_q
 510 denotes the rate constant (unknown) governing reaction q . Model equations were gen-
 511 erated in the C-programming language using the UNIVERSAL code generator, starting
 512 from an text-based input file (available in supplemental materials). UNIVERSAL, an open
 513 source Objective-C/Java code generator, is freely available as a Google Code project
 514 (<http://code.google.com/p/universal-code-generator/>). Model equations were solved us-
 515 ing the CVODE solver in the SUNDIALS library [38] on an Apple workstation (Apple,
 516 Cupertino, CA; OS X v10.6.8).

517 We ran the model to steady-state before calculating the response to DHT or growth
 518 factor inputs. The steady-state was estimated numerically by repeatedly solving the model

519 equations and estimating the difference between subsequent time points:

$$\|\mathbf{x}(t + \Delta t) - \mathbf{x}(t)\|_2 \leq \gamma \quad (3)$$

520 The quantities $\mathbf{x}(t)$ and $\mathbf{x}(t + \Delta t)$ denote the simulated abundance vector at time t and
521 $t + \Delta t$, respectively. The L_2 vector-norm was used as the distance metric, where $\Delta t = 100$
522 hr of simulated time and $\gamma = 0.001$ for all simulations.

523 We estimated an ensemble of model parameter sets using the Pareto Optimal En-
524 semble Techniques (POETs) multiobjective optimization routine [49, 83, 84]. POETs min-
525 imized the residual between model simulations and 43 separate training objectives taken
526 from protein and mRNA signaling data generated in androgen dependent, intermediate
527 and independent LNCaP cell lines (Table T1). From these training objectives, POETs
528 generated $> 10^6$ candidate parameter vectors from which we selected $N = 5000$ Pareto
529 rank-zero vectors for further analysis. The set-to-set correlation between selected sets
530 was approximately 0.60, suggesting only modest similarity between ensemble members.
531 Approximately 33%, or 560 of the 1674 parameters had a coefficient of variation (CV) of
532 less than 1.0, where the CV ranged from 0.59 to 5.8 over the ensemble. Details of the
533 parameter estimation problem and POETs are given in the supplemental materials.

534 **Sensitivity and robustness analysis.** Steady-state sensitivity coefficients were calcu-
535 lated for $N = 500$ parameter sets selected from the ensemble by solving the augmented
536 kinetic-sensitivity equations [19]:

$$\begin{bmatrix} \mathbf{S} \cdot \mathbf{r}(\mathbf{x}, \mathbf{k}) \\ \mathbf{A}(t_s) \mathbf{s}_j + \mathbf{b}_j(t_s) \end{bmatrix} = \begin{pmatrix} \mathbf{0} \\ \mathbf{0} \end{pmatrix} \quad j = 1, 2, \dots, \mathcal{P} \quad (4)$$

537 where

$$s_{ij}(t_s) = \frac{\partial x_i}{\partial k_j} \Big|_{t_s} \quad (5)$$

538 for each parameter set. Steady-state was calculated as described previously. The quan-
 539 tity j denotes the parameter index, \mathbf{A} denotes the Jacobian matrix, and \mathcal{P} denotes the
 540 number of parameters in the model. The vector \mathbf{b}_j denotes the j th column of the matrix
 541 of first-derivatives of the mass balances with respect to the parameters. Steady-state
 542 sensitivity coefficients were used because of the computational burden associated with
 543 sampling several hundred parameters sets for each of the 1674 parameters. The steady-
 544 state sensitivity coefficients $\mathcal{N}_{ij} \equiv s_{ij}$ were organized into an array for each parameter set
 545 in the ensemble:

$$\mathcal{N}^{(\epsilon)} = \begin{pmatrix} \mathcal{N}_{11}^{(\epsilon)} & \mathcal{N}_{12}^{(\epsilon)} & \dots & \mathcal{N}_{1j}^{(\epsilon)} & \dots & \mathcal{N}_{1P}^{(\epsilon)} \\ \mathcal{N}_{21}^{(\epsilon)} & \mathcal{N}_{22}^{(\epsilon)} & \dots & \mathcal{N}_{2j}^{(\epsilon)} & \dots & \mathcal{N}_{2P}^{(\epsilon)} \\ \vdots & \vdots & & \vdots & & \vdots \\ \mathcal{N}_{M1}^{(\epsilon)} & \mathcal{N}_{M2}^{(\epsilon)} & \dots & \mathcal{N}_{Mj}^{(\epsilon)} & \dots & \mathcal{N}_{MP}^{(\epsilon)} \end{pmatrix} \quad \epsilon = 1, 2, \dots, N_\epsilon \quad (6)$$

546 where ϵ denotes the index of the ensemble member, P denotes the number of parameters,
 547 N_ϵ denotes the number of parameter sets sampled ($N = 500$) and M denotes the number
 548 of model species. To estimate the relative fragility or robustness of species and reactions
 549 in the network, we decomposed $\mathcal{N}^{(\epsilon)}$ using Singular Value Decomposition (SVD):

$$\mathcal{N}^{(\epsilon)} = \mathbf{U}^{(\epsilon)} \Sigma^{(\epsilon)} \mathbf{V}^{T,(\epsilon)} \quad (7)$$

550 Coefficients of the left singular vectors corresponding to largest $\theta \leq 15$ singular values of
 551 $\mathcal{N}^{(\epsilon)}$ were rank-ordered to estimate important species combinations, while coefficients of
 552 the right singular vectors were used to rank important reaction combinations. Only coeffi-
 553 cients with magnitude greater than a threshold ($\delta = 0.001$) were considered. The fraction

554 of the θ vectors in which a reaction or species index occurred was used to quantify its
555 importance (sensitivity ranking). We compared the sensitivity ranking between different
556 conditions to understand how control in the network shifted in different cellular environ-
557 ments.

558 Robustness coefficients were calculated as shown previously [90]. Robustness coef-
559 ficients denoted by $\alpha(i, j, t_o, t_f)$ are defined as:

$$\alpha(i, j, t_o, t_f) = \left(\int_{t_o}^{t_f} x_i(t) dt \right)^{-1} \left(\int_{t_o}^{t_f} x_i^{(j)}(t) dt \right) \quad (8)$$

560 Robustness coefficients quantify the response of a marker to a structural or operational
561 perturbation to the network architecture. Here t_o and t_f denote the initial and final sim-
562 ulation time respectively, while i and j denote the indices for the marker and the pertur-
563 bation respectively. A value of $\alpha(i, j, t_o, t_f) > 1$, indicates increased marker abundance,
564 while $\alpha(i, j, t_o, t_f) < 1$ indicates decreased marker abundance following perturbation j . If
565 $\alpha(i, j, t_o, t_f) \sim 1$ the j th perturbation does not influence the abundance of marker i . Ro-
566 bustness coefficients were calculated (starting from steady-state) from $t_o = 0$ hr to $t_f = 72$
567 hr following the addition of 10nM DHT at t_o . Robustness coefficients were calculated for
568 the same $N = 500$ models selected for sensitivity analysis.

569 **Experimental Validation.**

570 **Cell culture and treatments** Androgen dependent LNCaP prostate cancer cells were
571 a gift from Dr. Brian Kirby (Cornell University), and the Castrate Resistant C4-2 prostate
572 cancer cell line was purchased from MD Anderson Cancer Center, University of Texas.
573 Cell lines were maintained in RPMI 1640 media (Life Technologies, Inc., Grand Island,
574 NY) with 10% fetal calf serum (FBS; Hyclone) and 1x antibiotic/antimycotic (Sigma, St.
575 Louis, MO) in a 5% CO₂ humidified atmosphere at 37°C. The AR inhibitor MDV3100
576 (enzalutamide) and the Raf inhibitor sorafenib were purchased from SantaCruz Biotech-

577 nology (Santa Cruz, CA). The PI3K inhibitor LY294002 was purchased from Cell Signaling
578 Technologies (Danvers, MA, USA). All stock solutions were diluted in DMSO (Sigma, St.
579 Louis, MO).

580 **Protein Extraction and Western Blot** LNCaP and C4-2 cells were seeded in 60 mm
581 dishes at a density of 4×10^5 . After 96 and 72 hrs, for LNCaP and C4-2 cells respec-
582 tively, the media was replaced with fresh media and drug treatments were added. After
583 24 hours, cells were washed twice in PBS buffer, scraped in 250 μ L ice-cold lysis buffer
584 (Pierce, Rockford, IL) supplemented with protease and phosphatase inhibitors (Sigma,
585 St. Louis, MO), and lysed for 30 min on ice. Lysates were centrifuged at 13,000 rpm
586 for 30 min at 4°C. After quantification of total protein by BCA assay, equal amounts of
587 total protein lysates (25 μ g) were resolved by SDS-PAGE and transferred onto PVDF
588 membranes. Membranes were blocked in 5% fat free milk and then probed with anti-
589 bodies. The primary antibodies used for western blot analysis were pAKT Ser473, AKT,
590 pS6 Ser240/244 , pERK Thr202/Tyr204, ERK, AR, and GAPDH were from Cell Signal-
591 ing Technologies (Danvers, MA, USA). For detection, enhanced chemiluminescence ECL
592 reagent (GE Healthcare, Pittsburgh, PA) was used and signals were visualized using the
593 ChemiDoc XRS system (Bio-Rad).

594 **MTT Assay** LNCaP and C4-2 cells were seeded at a density of 1×10^4 cells per well in 96
595 well plates. After 48 hrs the media was refreshed and drug treatments added. Cell growth
596 at 24, 48, and 72 hrs was determined using a 3-(4,5-dimethyl thiazol-2-yl)-2,5-diphenyl
597 tetrazolium bromide (MTT) assay. At the specified time point 10 μ MTT reagent (stock of
598 5 mg/mL in PBS) was added to each well and the cells were further incubated for 4 hrs.
599 At 4 hrs, the media was removed and 50 μ L of dissolving reagent DMSO was added to
600 each well. After an additional 10 min incubation, the absorbance was measured at 540
601 nm on a microplate reader. Each reading was adjusted by subtracting the absorbance
602 value for the blank (media only) and the results were then scaled to the DMSO-treated

603 (control) case.

604 **Acknowledgements**

605 This study was supported by award number U54CA143876 from the National Cancer
606 Institute. The content is solely the responsibility of the authors and does not necessarily
607 represent the official views of the National Cancer Institute or the National Institutes of
608 Health. This study was also supported by the National Science Foundation GK12 award
609 number DGE-1045513.

610 **References**

- 611 1. Abramoff M Magelhaes P RS (2004) Image processing with imagej. *Biophotonics*
612 *Int* **11**: 36–42
- 613 2. Aranda A, Pascual A (2001) Nuclear and Hormone Receptors and Gene Expression.
614 *Physiological Reviews* **81**: 1269–1304
- 615 3. Attard G, de Bono JS (2009) Prostate cancer: PSA as an intermediate end point in
616 clinical trials. *Nat Rev Urol* **6**: 473–5
- 617 4. Brinkmann AO, Blok LJ, de Ruiter PE, Doesburg P, Steketee K, Berrevoets CA, Trap-
618 man J (1999) Mechanisms of androgen receptor activation and function. *J Steroid
619 Biochem Mol Biol* **69**: 307–13
- 620 5. Brown KS, Sethna JP (2003) Statistical mechanical approaches to models with
621 many poorly known parameters. *Phys Rev E Stat Nonlin Soft Matter Phys* **68**:
622 021904
- 623 6. Brunet A, Bonni A, Zigmond MJ, Lin MZ, Juo P, Hu LS, Anderson MJ, Arden KC,
624 Blenis J, Greenberg ME (1999) Akt promotes cell survival by phosphorylating and
625 inhibiting a Forkhead transcription factor. *Cell* **96**: 857–68
- 626 7. Busà R, Paronetto MP, Farini D, Pierantozzi E, Botti F, Angelini DF, Attisani F, Ves-
627 pasiani G, Sette C (2007) The RNA-binding protein Sam68 contributes to prolifera-
628 tion and survival of human prostate cancer cells. *Oncogene* **26**: 4372–82
- 629 8. Cai C, Portnoy DC, Wang H, Jiang X, Chen S, Balk SP (2009) Androgen receptor
630 expression in prostate cancer cells is suppressed by activation of epidermal growth
631 factor receptor and ErbB2. *Cancer Res* **69**: 5202–9
- 632 9. Cardillo MR, Monti S, Di Silverio F, Gentile V, Sciarra F, Toscano V (2003) Insulin-like
633 growth factor (IGF)-I, IGF-II and IGF type I receptor (IGFR-I) expression in prostatic
634 cancer. *Anticancer Res* **23**: 3825–35
- 635 10. Chen L, Mooso BA, Jathal MK, Madhav A, Johnson SD, van Spyk E, Mikhailova M,

- 636 Zierenberg-Ripoll A, Xue L, Vinall RL, deVere White RW, Ghosh PM (2011) Dual
637 EGFR/HER2 inhibition sensitizes prostate cancer cells to androgen withdrawal by
638 suppressing ErbB3. *Clin Cancer Res* **17**: 6218–28
- 639 11. Chen S, Kesler CT, Paschal BM, Balk SP (2009) Androgen receptor phosphorylation
640 and activity are regulated by an association with protein phosphatase 1. *J Biol Chem*
641 **284**: 25576–84
- 642 12. Chiu YT, Han HY, Leung SCL, Yuen HF, Chau CW, Guo Z, Qiu Y, Chan KW, Wang X,
643 Wong YC, Ling MT (2009) CDC25A functions as a novel Ar corepressor in prostate
644 cancer cells. *J Mol Biol* **385**: 446–56
- 645 13. Chuang TD, Chen SJ, Lin FF, Veeramani S, Kumar S, Batra SK, Tu Y, Lin MF (2010)
646 Human prostatic acid phosphatase, an authentic tyrosine phosphatase, dephospho-
647 rylates ErbB-2 and regulates prostate cancer cell growth. *J Biol Chem* **285**: 23598–
648 606
- 649 14. Cinar B, De Benedetti A, Freeman MR (2005) Post-transcriptional regulation of the
650 androgen receptor by Mammalian target of rapamycin. *Cancer Res* **65**: 2547–53
- 651 15. Craft N, Shostak Y, Carey M, Sawyers CL (1999) A mechanism for hormone-
652 independent prostate cancer through modulation of androgen receptor signaling by
653 the HER-2/neu tyrosine kinase. *Nat Med* **5**: 280–5
- 654 16. Dahut WL, Scripture C, Posadas E, Jain L, Gulley JL, Arlen PM, Wright JJ, Yu Y, Cao
655 L, Steinberg SM, Aragon-Ching JB, Venitz J, Jones E, Chen CC, Figg WD (2008)
656 A phase II clinical trial of sorafenib in androgen-independent prostate cancer. *Clin
657 Cancer Res* **14**: 209–14
- 658 17. Davis JN, Wojno KJ, Daignault S, Hofer MD, Kuefer R, Rubin MA, Day ML (2006)
659 Elevated E2F1 inhibits transcription of the androgen receptor in metastatic hormone-
660 resistant prostate cancer. *Cancer Res* **66**: 11897–906
- 661 18. de Bono JS, Oudard S, Ozguroglu M, Hansen S, Machiels JP, Kocak I, Gravis G, Bo-

- drogi I, Mackenzie MJ, Shen L, Roessner M, Gupta S, Sartor AO, TROPIC Investigators (2010) Prednisone plus cabazitaxel or mitoxantrone for metastatic castration-resistant prostate cancer progressing after docetaxel treatment: a randomised open-label trial. *Lancet* **376**: 1147–54
19. Dickinson R, Gelinas R (1976) Sensitivity analysis of ordinary differential equation systems—A direct method. *Journal of Computational Physics* **21**: 123–143
20. Fang Z, Zhang T, Dizeyi N, Chen S, Wang H, Swanson KD, Cai C, Balk SP, Yuan X (2012) Androgen Receptor Enhances p27 Degradation in Prostate Cancer Cells through Rapid and Selective TORC2 Activation. *J Biol Chem* **287**: 2090–8
21. Feldman BJ, Feldman D (2001) The development of androgen-independent prostate cancer. *Nat Rev Cancer* **1**: 34–45
22. Fonseca C FP (1993) Genetic algorithms for multiobjective optimization: Formulation, discussion and generalization. In *Proceedings of the fifth international conference on genetic algorithms Citeseer* **423**: 416–423
23. Gadkar KG, Doyle 3rd FJ, Crowley TJ, Varner JD (2003) Cybernetic model predictive control of a continuous bioreactor with cell recycle. *Biotechnol Prog* **19**: 1487–97
24. Gioeli D, Paschal BM (2012) Post-translational modification of the androgen receptor. *Mol Cell Endocrinol* **352**: 70–8
25. Graff JR, Konicek BW, Lynch RL, Dumstorf CA, Dowless MS, McNulty AM, Parsons SH, Brail LH, Colligan BM, Koop JW, Hurst BM, Deddens JA, Neubauer BL, Stanacato LF, Carter HW, Douglass LE, Carter JH (2009) eIF4E activation is commonly elevated in advanced human prostate cancers and significantly related to reduced patient survival. *Cancer Res* **69**: 3866–73
26. Graff JR, Konicek BW, McNulty AM, Wang Z, Houck K, Allen S, Paul JD, Hbaiu A, Goode RG, Sandusky GE, Vessella RL, Neubauer BL (2000) Increased AKT activity contributes to prostate cancer progression by dramatically accelerating prostate

- 688 tumor growth and diminishing p27Kip1 expression. *J Biol Chem* **275**: 24500–5
- 689 27. Gregory CW, Fei X, Ponguta LA, He B, Bill HM, French FS, Wilson EM (2004) Epi-
690 dermal growth factor increases coactivation of the androgen receptor in recurrent
691 prostate cancer. *J Biol Chem* **279**: 7119–30
- 692 28. Gregory CW, He B, Johnson RT, Ford OH, Mohler JL, French FS, Wilson EM (2001)
693 A mechanism for androgen receptor-mediated prostate cancer recurrence after an-
694 drogen deprivation therapy. *Cancer Res* **61**: 4315–9
- 695 29. Guo Z, Dai B, Jiang T, Xu K, Xie Y, Kim O, Nesheiwat I, Kong X, Melamed J, Han-
696 dratta VD, Njar VCO, Brodie AMH, Yu LR, Veenstra TD, Chen H, Qiu Y (2006) Reg-
697 ulation of androgen receptor activity by tyrosine phosphorylation. *Cancer Cell* **10**:
698 309–19
- 699 30. Ha S, Ruoff R, Kahoud N, Franke TF, Logan SK (2011) Androgen receptor levels
700 are upregulated by Akt in prostate cancer. *Endocr Relat Cancer* **18**: 245–55
- 701 31. Hakariya T, Shida Y, Sakai H, Kanetake H, Igawa T (2006) EGFR signaling path-
702 way negatively regulates PSA expression and secretion via the PI3K-Akt pathway in
703 LNCaP prostate cancer cells. *Biochem Biophys Res Commun* **342**: 92–100
- 704 32. Handl J, Kell DB, Knowles J (2007) Multiobjective optimization in bioinformatics and
705 computational biology. *IEEEACM Trans Comput Biol Bioinform* **4**: 279–92
- 706 33. Harris WP, Mostaghel EA, Nelson PS, Montgomery B (2009) Androgen deprivation
707 therapy: progress in understanding mechanisms of resistance and optimizing an-
708 drogen depletion. *Nat Clin Pract Urol* **6**: 76–85
- 709 34. Heemers HV, Tindall DJ (2007) Androgen receptor (AR) coregulators: a diversity of
710 functions converging on and regulating the AR transcriptional complex. *Endocr Rev*
711 **28**: 778–808
- 712 35. Heinlein CA, Chang C (2002) Androgen receptor (AR) coregulators: an overview.
713 *Endocr Rev* **23**: 175–200

- 714 36. Heinlein CA, Chang C (2004) Androgen receptor in prostate cancer. *Endocr Rev* **25**:
715 276–308
- 716 37. Hendriks BS, Opresko LK, Wiley HS, Lauffenburger D (2003) Quantitative analysis
717 of HER2-mediated effects on HER2 and epidermal growth factor receptor endocytosis:
718 distribution of homo- and heterodimers depends on relative HER2 levels. *J Biol
719 Chem* **278**: 23343–51
- 720 38. Hindmarsh A, Brown P, Grant K, Lee S, Serban R, Shumaker D, Woodward C
721 (2005) SUNDIALS: Suite of nonlinear and differential/algebraic equation solvers.
722 *ACM Transactions on Mathematical Software* **31**: 363–396
- 723 39. Hoffman RM (2011) Clinical practice. Screening for prostate cancer. *N Engl J Med*
724 **365**: 2013–9
- 725 40. Horoszewicz JS, Leong SS, Kawinski E, Karr JP, Rosenthal H, Chu TM, Mirand EA,
726 Murphy GP (1983) LNCaP model of human prostatic carcinoma. *Cancer Res* **43**:
727 1809–18
- 728 41. Huggins C (1967) Endocrine-induced regression of cancers. *Cancer Res* **27**: 1925–
729 30
- 730 42. Igawa T, Lin FF, Lee MS, Karan D, Batra SK, Lin MF (2002) Establishment and char-
731 acterization of androgen-independent human prostate cancer LNCaP cell model.
732 *Prostate* **50**: 222–35
- 733 43. Kantoff PW, Higano CS, Shore ND, Berger ER, Small EJ, Penson DF, Red-
734 fern CH, Ferrari AC, Dreicer R, Sims RB, Xu Y, Frohlich MW, Schellhammer PF,
735 IMPACT Study Investigators (2010) Sipuleucel-T immunotherapy for castration-
736 resistant prostate cancer. *N Engl J Med* **363**: 411–22
- 737 44. Karantanos T, Corn PG, Thompson TC (2013) Prostate cancer progression after
738 androgen deprivation therapy: mechanisms of castrate resistance and novel thera-
739 peutic approaches. *Oncogene*

- 740 45. Knudsen KE, Arden KC, Cavenee WK (1998) Multiple G1 regulatory elements con-
741 trol the androgen-dependent proliferation of prostatic carcinoma cells. *J Biol Chem*
742 **273**: 20213–22
- 743 46. Lapenna S, Giordano A (2009) Cell cycle kinases as therapeutic targets for cancer.
744 *Nat Rev Drug Discov* **8**: 547–66
- 745 47. Lee MS, Igawa T, Lin MF (2004) Tyrosine-317 of p52(Shc) mediates androgen-
746 stimulated proliferation signals in human prostate cancer cells. *Oncogene* **23**: 3048–
747 58
- 748 48. Lee MS, Igawa T, Yuan TC, Zhang XQ, Lin FF, Lin MF (2003) ErbB-2 signaling
749 is involved in regulating PSA secretion in androgen-independent human prostate
750 cancer LNCaP C-81 cells. *Oncogene* **22**: 781–96
- 751 49. Lequieu J, Chakrabarti A, Nayak S, Varner JD (2011) Computational modeling and
752 analysis of insulin induced eukaryotic translation initiation. *PLoS Comput Biol* **7**:
753 e1002263
- 754 50. Lim JTE, Mansukhani M, Weinstein IB (2005) Cyclin-dependent kinase 6 associates
755 with the androgen receptor and enhances its transcriptional activity in prostate can-
756 cer cells. *Proc Natl Acad Sci U S A* **102**: 5156–61
- 757 51. Lin HK, Hu YC, Yang L, Altuwaijri S, Chen YT, Kang HY, Chang C (2003) Suppres-
758 sion versus induction of androgen receptor functions by the phosphatidylinositol 3-
759 kinase/Akt pathway in prostate cancer LNCaP cells with different passage numbers.
760 *J Biol Chem* **278**: 50902–7
- 761 52. Lin HK, Yeh S, Kang HY, Chang C (2001) Akt suppresses androgen-induced apop-
762 tosis by phosphorylating and inhibiting androgen receptor. *Proc Natl Acad Sci U S*
763 **A** **98**: 7200–5
- 764 53. Lin MF, Lee MS, Garcia-Arenas R, Lin FF (2000) Differential responsiveness of pro-
765 static acid phosphatase and prostate-specific antigen mRNA to androgen in prostate

- 766 cancer cells. *Cell Biol Int* **24**: 681–9
- 767 54. Lin MF, Lee MS, Zhou XW, Andressen JC, Meng TC, Johansson SL, West WW,
768 Taylor RJ, Anderson JR, Lin FF (2001) Decreased expression of cellular prostatic
769 acid phosphatase increases tumorigenicity of human prostate cancer cells. *J Urol*
770 **166**: 1943–50
- 771 55. Lindemann RK, Braig M, Ballschmieter P, Guise TA, Nordheim A, Dittmer J (2003)
772 Protein kinase Calpha regulates Ets1 transcriptional activity in invasive breast can-
773 cer cells. *Int J Oncol* **22**: 799–805
- 774 56. Liu G, Chen YH, Kolesar J, Huang W, Dipaola R, Pins M, Carducci M, Stein M,
775 Bubley GJ, Wilding G (2013) Eastern Cooperative Oncology Group Phase II Trial of
776 lapatinib in men with biochemically relapsed, androgen dependent prostate cancer.
777 *Urol Oncol* **31**: 211–8
- 778 57. Liu Y, Majumder S, McCall W, Sartor CI, Mohler JL, Gregory CW, Earp HS, Whang
779 YE (2005) Inhibition of HER-2/neu kinase impairs androgen receptor recruitment to
780 the androgen responsive enhancer. *Cancer Res* **65**: 3404–9
- 781 58. Lu S, Tsai SY, Tsai MJ (1997) Regulation of androgen-dependent prostatic cancer
782 cell growth: androgen regulation of CDK2, CDK4, and CKI p16 genes. *Cancer Res*
783 **57**: 4511–6
- 784 59. Mangelsdorf DJ, Thummel C, Beato M, Herrlich P, Schütz G, Umesono K, Blum-
785 berg B, Kastner P, Mark M, Chambon P, Evans RM (1995) The nuclear receptor
786 superfamily: the second decade. *Cell* **83**: 835–9
- 787 60. Medema RH, Kops GJ, Bos JL, Burgener BM (2000) AFX-like Forkhead transcrip-
788 tion factors mediate cell-cycle regulation by Ras and PKB through p27kip1. *Nature*
789 **404**: 782–7
- 790 61. Meng TC, Lee MS, Lin MF (2000) Interaction between protein tyrosine phosphatase
791 and protein tyrosine kinase is involved in androgen-promoted growth of human

- 792 prostate cancer cells. *Oncogene* **19**: 2664–77
- 793 62. Moles CG, Mendes P, Banga JR (2003) Parameter estimation in biochemical path-
794 ways: a comparison of global optimization methods. *Genome Res* **13**: 2467–74
- 795 63. Moyer VA, U.S. Preventive Services Task Force (2012) Screening for prostate can-
796 cer: U.S. Preventive Services Task Force recommendation statement. *Ann Intern
797 Med* **157**: 120–34
- 798 64. Murillo H, Huang H, Schmidt LJ, Smith DI, Tindall DJ (2001) Role of PI3K signaling in
799 survival and progression of LNCaP prostate cancer cells to the androgen refractory
800 state. *Endocrinology* **142**: 4795–805
- 801 65. Ngan ESW, Hashimoto Y, Ma ZQ, Tsai MJ, Tsai SY (2003) Overexpression of
802 Cdc25B, an androgen receptor coactivator, in prostate cancer. *Oncogene* **22**: 734–9
- 803 66. Parker C, Nilsson S, Heinrich D, Helle SI, O’Sullivan JM, Fosså SD, Chodacki A,
804 Wiechno P, Logue J, Seke M, Widmark A, Johannessen DC, Hoskin P, Bottomley
805 D, James ND, Solberg A, Syndikus I, Kliment J, Wedel S, Boehmer S, et al (2013)
806 Alpha emitter radium-223 and survival in metastatic prostate cancer. *N Engl J Med*
807 **369**: 213–23
- 808 67. Paronetto MP, Cappellari M, Busà R, Pedrotti S, Vitali R, Comstock C, Hyslop T,
809 Knudsen KE, Sette C (2010) Alternative splicing of the cyclin D1 proto-oncogene is
810 regulated by the RNA-binding protein Sam68. *Cancer Res* **70**: 229–39
- 811 68. Perry JE, Grossmann ME, Tindall DJ (1998) Epidermal growth factor induces cyclin
812 D1 in a human prostate cancer cell line. *Prostate* **35**: 117–24
- 813 69. Petre-Draviam CE, Cook SL, Burd CJ, Marshall TW, Wetherill YB, Knudsen KE
814 (2003) Specificity of cyclin D1 for androgen receptor regulation. *Cancer Res* **63**:
815 4903–13
- 816 70. Ponguta LA, Gregory CW, French FS, Wilson EM (2008) Site-specific androgen
817 receptor serine phosphorylation linked to epidermal growth factor-dependent growth

- 818 of castration-recurrent prostate cancer. *J Biol Chem* **283**: 20989–1001
- 819 71. Pratt WB, Toft DO (1997) Steroid receptor interactions with heat shock protein and
820 immunophilin chaperones. *Endocr Rev* **18**: 306–60
- 821 72. Prescott J, Coetzee GA (2006) Molecular chaperones throughout the life cycle of
822 the androgen receptor. *Cancer Lett* **231**: 12–9
- 823 73. Rodríguez-Ubreva FJ, Cariaga-Martinez AE, Cortés MA, Romero-De Pablos M,
824 Ropero S, López-Ruiz P, Colás B (2010) Knockdown of protein tyrosine phos-
825 phatase SHP-1 inhibits G1/S progression in prostate cancer cells through the regu-
826 lation of components of the cell-cycle machinery. *Oncogene* **29**: 345–55
- 827 74. Sartor O, Pal SK (2013) Abiraterone and its place in the treatment of metastatic
828 CRPC. *Nat Rev Clin Oncol* **10**: 6–8
- 829 75. Sato N, Sadar MD, Bruchovsky N, Saatcioglu F, Rennie PS, Sato S, Lange PH,
830 Gleave ME (1997) Androgenic induction of prostate-specific antigen gene is re-
831 pressed by protein-protein interaction between the androgen receptor and AP-1/c-
832 Jun in the human prostate cancer cell line LNCaP. *J Biol Chem* **272**: 17485–94
- 833 76. Scher HI, Fizazi K, Saad F, Taplin ME, Sternberg CN, Miller K, de Wit R, Mulders P,
834 Chi KN, Shore ND, Armstrong AJ, Flraig TW, Fléchon A, Mainwaring P, Fleming M,
835 Hainsworth JD, Hirmand M, Selby B, Seely L, de Bono JS, *et al* (2012) Increased
836 survival with enzalutamide in prostate cancer after chemotherapy. *N Engl J Med*
837 **367**: 1187–97
- 838 77. Seaton A, Scullin P, Maxwell PJ, Wilson C, Pettigrew J, Gallagher R, O'Sullivan
839 JM, Johnston PG, Waugh DJJ (2008) Interleukin-8 signaling promotes androgen-
840 independent proliferation of prostate cancer cells via induction of androgen receptor
841 expression and activation. *Carcinogenesis* **29**: 1148–56
- 842 78. Sharma A, Yeow WS, Ertel A, Coleman I, Clegg N, Thangavel C, Morrissey C, Zhang
843 X, Comstock CES, Witkiewicz AK, Gomella L, Knudsen ES, Nelson PS, Knudsen

- 844 KE (2010) The retinoblastoma tumor suppressor controls androgen signaling and
845 human prostate cancer progression. *J Clin Invest* **120**: 4478–92
- 846 79. Sherr CJ, Roberts JM (1999) CDK inhibitors: positive and negative regulators of
847 G1-phase progression. *Genes Dev* **13**: 1501–12
- 848 80. Siegel R, Naishadham D, Jemal A (2013) Cancer statistics, 2013. *CA Cancer J Clin*
849 **63**: 11–30
- 850 81. Slamon DJ, Godolphin W, Jones LA, Holt JA, Wong SG, Keith DE, Levin WJ, Stuart
851 SG, Udove J, Ullrich A (1989) Studies of the HER-2/neu proto-oncogene in human
852 breast and ovarian cancer. *Science* **244**: 707–12
- 853 82. Sobel RE, Sadar MD (2005) Cell lines used in prostate cancer research: a com-
854 pendium of old and new lines—part 1. *J Urol* **173**: 342–59
- 855 83. Song SO, Chakrabarti A, Varner JD (2010) Ensembles of signal transduction models
856 using Pareto Optimal Ensemble Techniques (POETs). *Biotechnol J* **5**: 768–80
- 857 84. Song SO, Varner J (2009) Modeling and analysis of the molecular basis of pain in
858 sensory neurons. *PLoS One* **4**: e6758
- 859 85. Takaishi H, Konishi H, Matsuzaki H, Ono Y, Shirai Y, Saito N, Kitamura T, Ogawa
860 W, Kasuga M, Kikkawa U, Nishizuka Y (1999) Regulation of nuclear translocation of
861 forkhead transcription factor AFX by protein kinase B. *Proc Natl Acad Sci U S A* **96**:
862 11836–41
- 863 86. Tam L, McGlynn LM, Traynor P, Mukherjee R, Bartlett JMS, Edwards J (2007) Ex-
864 pression levels of the JAK/STAT pathway in the transition from hormone-sensitive to
865 hormone-refractory prostate cancer. *Br J Cancer* **97**: 378–83
- 866 87. Taneja SS, Ha S, Swenson NK, Huang HY, Lee P, Melamed J, Shapiro E, Garabe-
867 dian MJ, Logan SK (2005) Cell-specific regulation of androgen receptor phosphory-
868 lation in vivo. *J Biol Chem* **280**: 40916–24
- 869 88. Tannock IF, de Wit R, Berry WR, Horti J, Pluzanska A, Chi KN, Oudard S, Théodore

- 870 C, James ND, Turesson I, Rosenthal MA, Eisenberger MA, TAX 327 Investigators
871 (2004) Docetaxel plus prednisone or mitoxantrone plus prednisone for advanced
872 prostate cancer. *N Engl J Med* **351**: 1502–12
- 873 89. Tasseff R, Nayak S, Salim S, Kaushik P, Rizvi N, Varner JD (2010) Analysis of the
874 molecular networks in androgen dependent and independent prostate cancer re-
875 vealed fragile and robust subsystems. *PLoS One* **5**: e8864
- 876 90. Tasseff R, Nayak S, Song SO, Yen A, Varner JD (2011) Modeling and analysis of
877 retinoic acid induced differentiation of uncommitted precursor cells. *Integr Biol Camb*
878 **3**: 578–91
- 879 91. Veeramani S, Igawa T, Yuan TC, Lin FF, Lee MS, Lin JS, Johansson SL, Lin
880 MF (2005) Expression of p66(Shc) protein correlates with proliferation of human
881 prostate cancer cells. *Oncogene* **24**: 7203–12
- 882 92. Veeramani S, Yuan TC, Chen SJ, Lin FF, Petersen JE, Shaheduzzaman S, Srivas-
883 tava S, MacDonald RG, Lin MF (2005) Cellular prostatic acid phosphatase: a pro-
884 tein tyrosine phosphatase involved in androgen-independent proliferation of prostate
885 cancer. *Endocr Relat Cancer* **12**: 805–22
- 886 93. Villaverde AF, Banga JR (2014) Reverse engineering and identification in systems
887 biology: strategies, perspectives and challenges. *J R Soc Interface* **11**: 20130505
- 888 94. Wayman J, Varner J (2013) Biological systems modeling of metabolic and signaling
889 networks. *Curr Opin Chem Eng* **2**: 365 – 372
- 890 95. Weber MJ, Gioeli D (2004) Ras signaling in prostate cancer progression. *J Cell*
891 *Biochem* **91**: 13–25
- 892 96. Wen Y, Hu MC, Makino K, Spohn B, Bartholomeusz G, Yan DH, Hung MC (2000)
893 HER-2/neu promotes androgen-independent survival and growth of prostate cancer
894 cells through the Akt pathway. *Cancer Res* **60**: 6841–5
- 895 97. Whang YE, Armstrong AJ, Rathmell WK, Godley PA, Kim WY, Pruthi RS, Wallen

- 896 EM, Crane JM, Moore DT, Grigson G, Morris K, Watkins CP, George DJ (2013) A
897 phase II study of lapatinib, a dual EGFR and HER-2 tyrosine kinase inhibitor, in
898 patients with castration-resistant prostate cancer. *Urol Oncol* **31**: 82–6
- 899 98. Wilkinson MG, Millar JB (2000) Control of the eukaryotic cell cycle by MAP kinase
900 signaling pathways. *FASEB J* **14**: 2147–57
- 901 99. Xu Y, Chen SY, Ross KN, Balk SP (2006) Androgens induce prostate cancer cell pro-
902 liferation through mammalian target of rapamycin activation and post-transcriptional
903 increases in cyclin D proteins. *Cancer Res* **66**: 7783–92
- 904 100. Yamamoto A, Hashimoto Y, Kohri K, Ogata E, Kato S, Ikeda K, Nakanishi M (2000)
905 Cyclin E as a coactivator of the androgen receptor. *J Cell Biol* **150**: 873–80
- 906 101. Yeh S, Lin HK, Kang HY, Thin TH, Lin MF, Chang C (1999) From HER2/Neu signal
907 cascade to androgen receptor and its coactivators: a novel pathway by induction of
908 androgen target genes through MAP kinase in prostate cancer cells. *Proc Natl Acad
909 Sci U S A* **96**: 5458–63
- 910 102. Yeh S, Miyamoto H, Nishimura K, Kang H, Ludlow J, Hsiao P, Wang C, Su C, Chang
911 C (1998) Retinoblastoma, a tumor suppressor, is a coactivator for the androgen
912 receptor in human prostate cancer DU145 cells. *Biochem Biophys Res Commun*
913 **248**: 361–7
- 914 103. Yuan TC, Lin FF, Veeramani S, Chen SJ, Earp 3rd HS, Lin MF (2007) ErbB-2 via
915 PYK2 upregulates the adhesive ability of androgen receptor-positive human prostate
916 cancer cells. *Oncogene* **26**: 7552–9

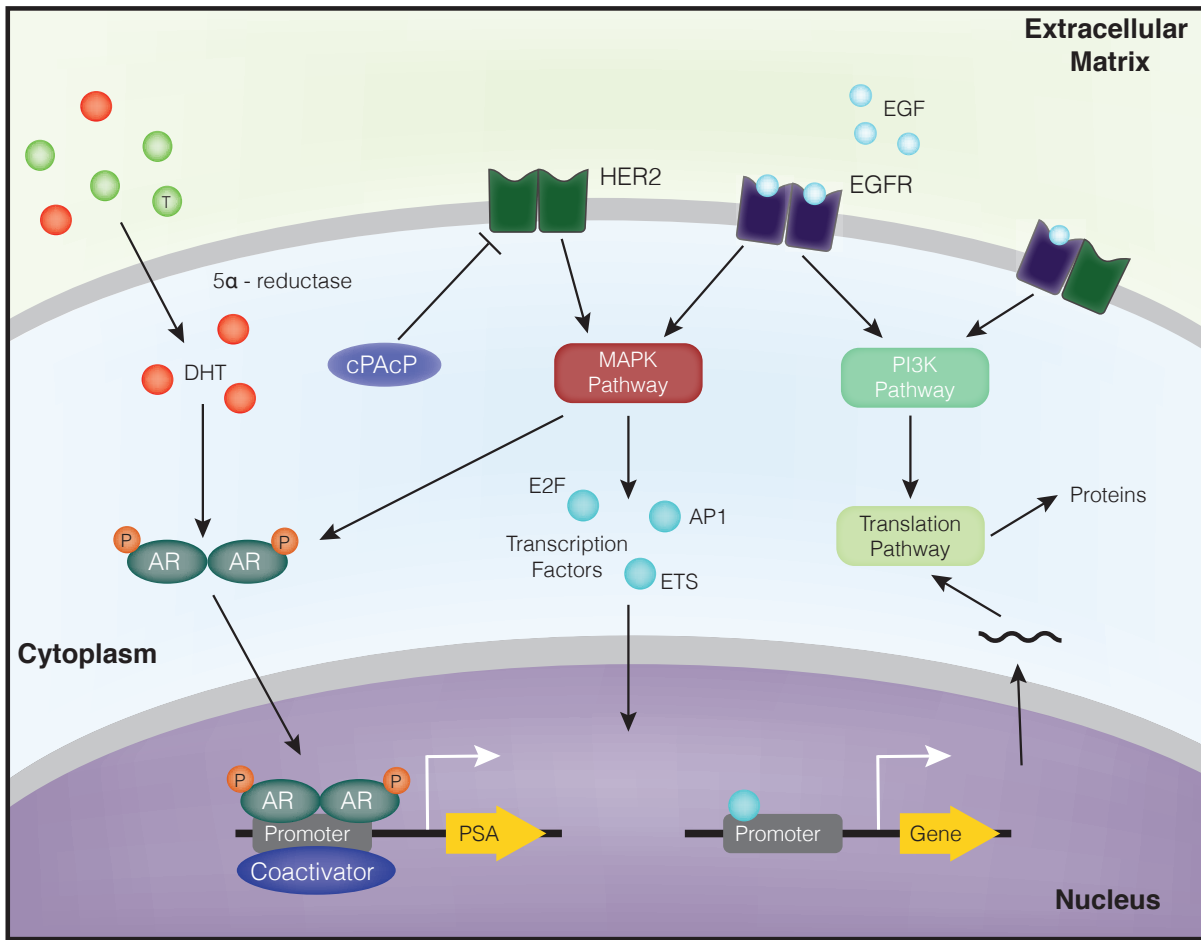


Fig. 1: Schematic overview of the prostate signaling network. The model describes hormone and growth factor induced expression of several proteins, including PSA. In the absence of outside hormones/growth factors, overactive HER2 can stimulate the MAPK and AKT pathways. AR can be activated directly by the MAPK pathway.

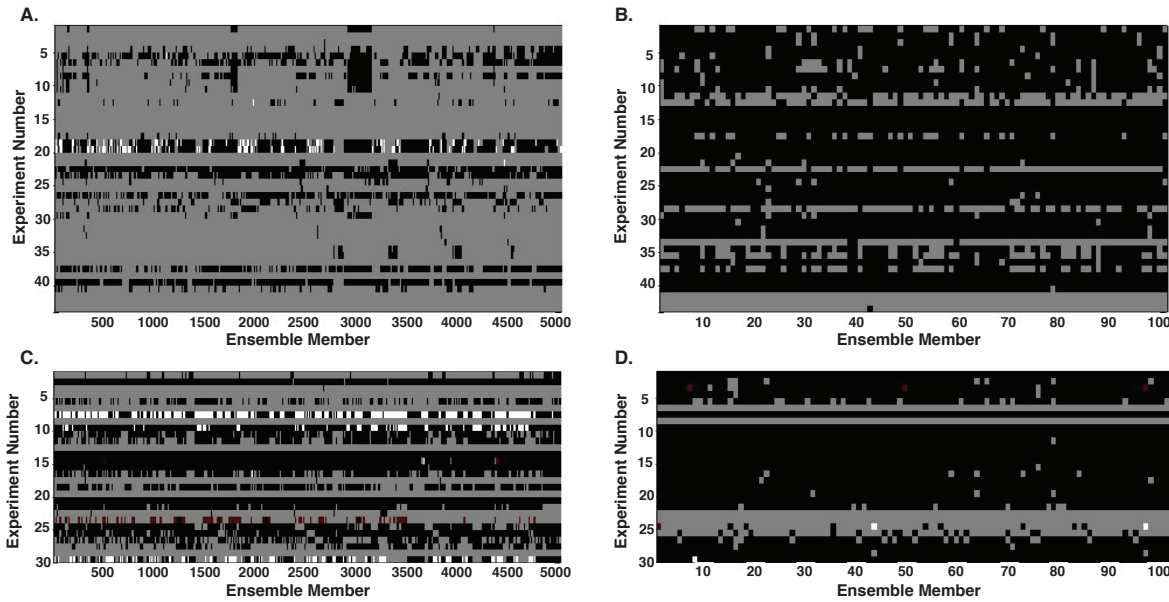


Fig. 2: Simulation results versus experimental results for training and validation data. Experiment numbers 1 through 43 were used for training, while experiments 44 through 72 were validation. Gray means the ensemble member qualitatively fit experimental data in both models. White means the ensemble member only fit the data using the new model that included HER2 heterodimerization. Red means the ensemble member fit using only the old model. Black corresponds to an incorrect cellular response in both models. A., C. Training and validation results, respectively, for entire ensemble population using both the original model and an updated model including HER2 heterodimerization ($N = 5000$). B., D. Simulation results for training and validation of a random set of 100 members using both models.

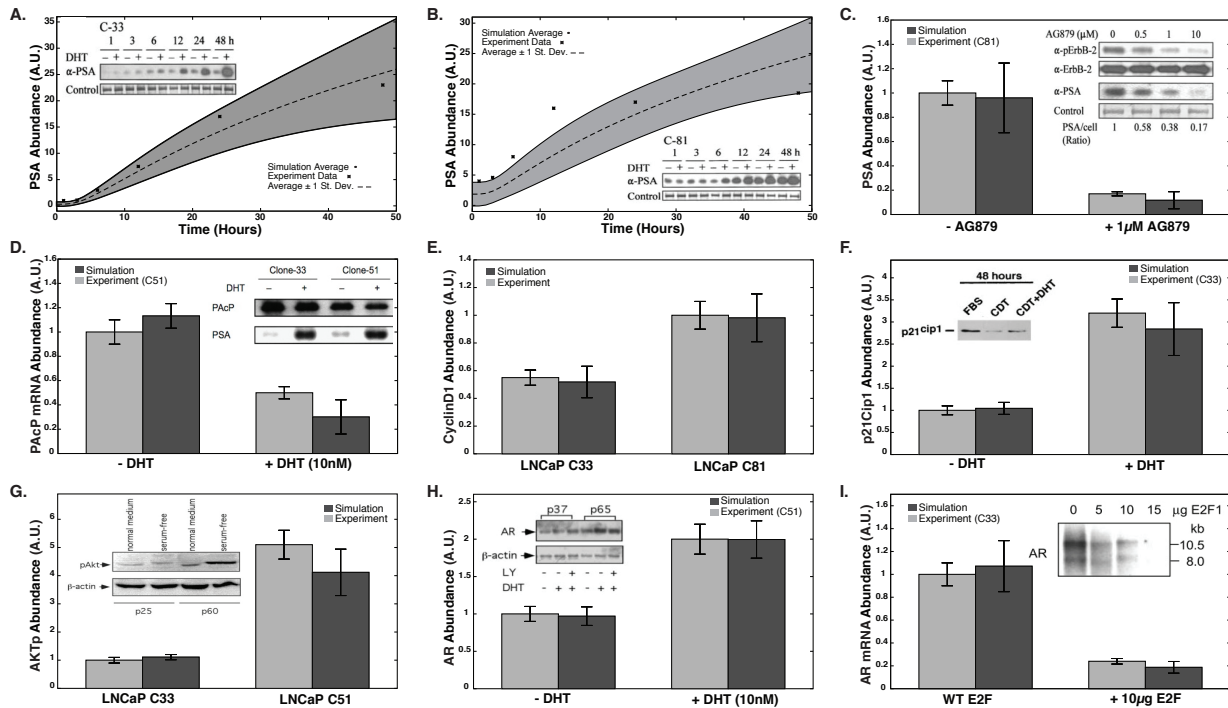


Fig. 3: Ensemble performance against selected training objectives ($N = 5000$). A, B. Time course data for PSA concentration due to a stimulus of 10 nM DHT in LNCaP C33 cells and LNCaP C81 cells, respectively (O₂, O₃). C. PSA levels in the presence and absence of a HER2 inhibitor (LNCaP C81 cells, O₇). D. PAcP mRNA levels at 72 hours in the presence and absence of DHT (LNCaP C51 cells, O₁₄). E. Steady-state cyclin D levels in LNCaP C33 vs. C81 (O₁₇). F. p21Cip1 levels at 48 hrs in the presence and absence of DHT (LNCaP C33, O₂₅). G. Steady-state AKT phosphorylation levels in LNCaP C33 vs. C51 (O₃₀). H. AR levels at 24 hours in the presence and absence of DHT (LNCaP C51, O₃₁). I. AR mRNA levels in the presence and absence of E2F over expression (LNCaP C33, O₃₄).

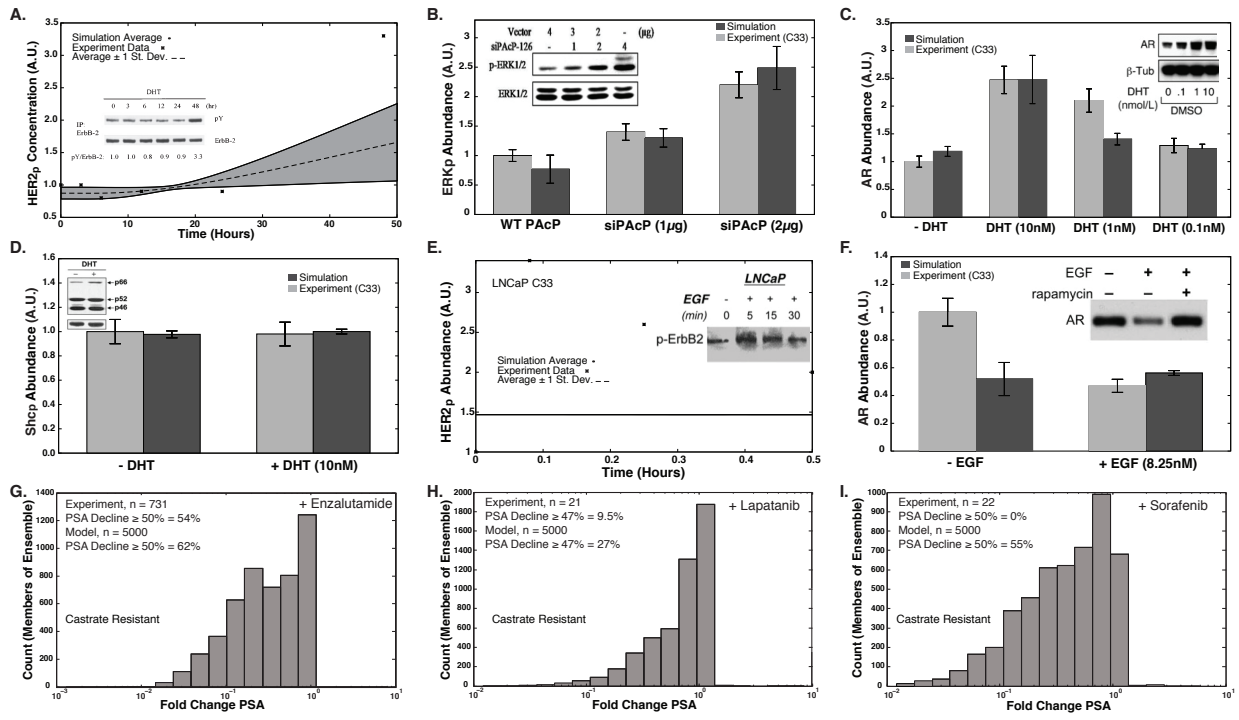


Fig. 4: Blind model predictions for the ensemble ($N = 5000$). The model ensemble's predictive ability was assessed by comparing simulation versus experimental data not used for training. A. Time course data for HER phosphorylation due to a stimulus of 10 nM DHT (LNCaP C33, P1). B. ERK phosphorylation levels in the presence and absence of a PAcP inhibitor (LNCaP C33 cells, P3). C. AR levels at 24 hrs in varying levels of DHT (LNCaP C33, P17). D. Shc phosphorylation levels at 24 hrs in the presence and absence of DHT (LNCaP C33, P22). E. Time course data for HER phosphorylation due to a stimulus of 1.6 nM EGF (LNCaP C33, P7). F. AR levels in varying levels of EGF (LNCaP C33, P14). G, H, I. Fold change in PSA concentration due to drug stimulus: enzalutamide, lapatinib, and sorafenib.

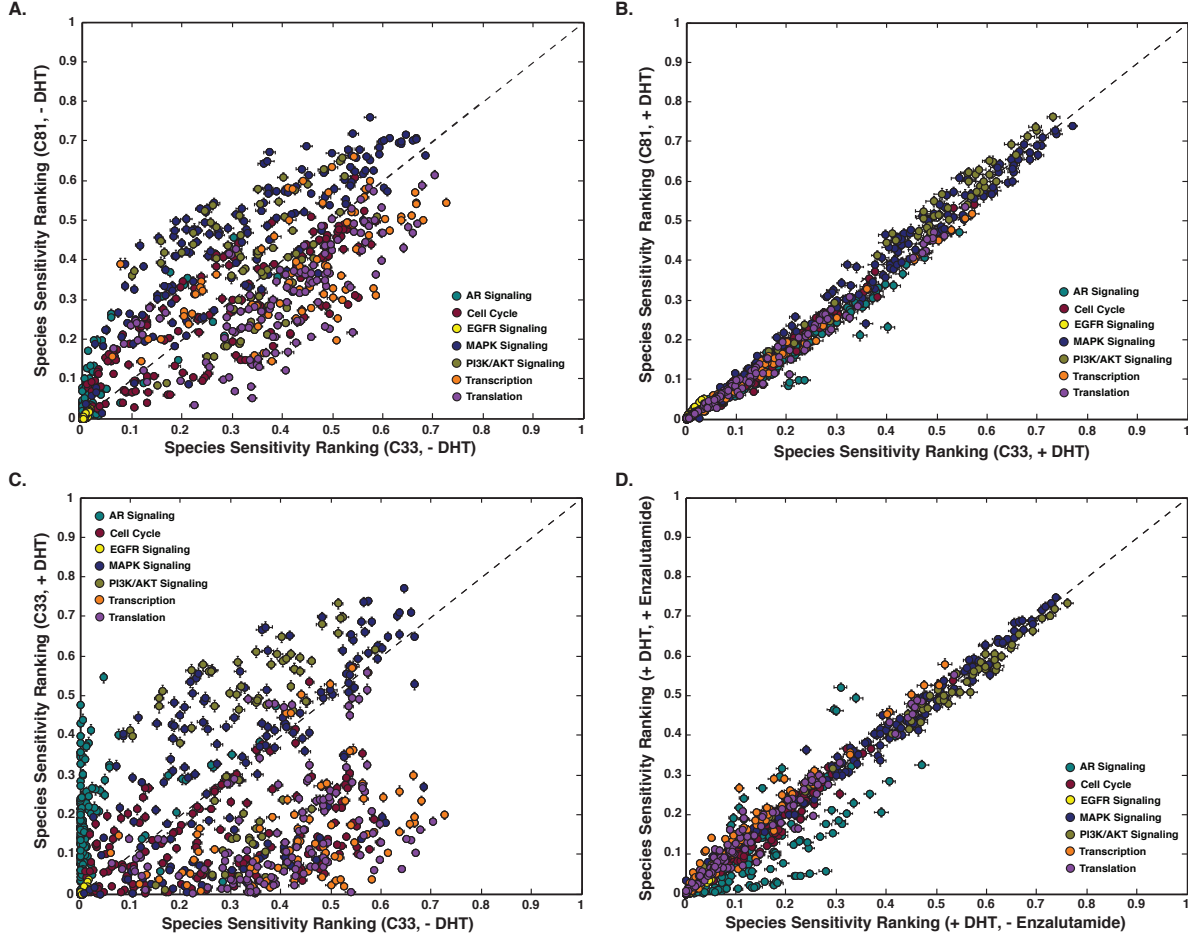


Fig. 5: Sensitivity analysis of a population of prostate models ($N = 500$). Species with a low sensitivity are considered robust, while species with a high sensitivity ranking are considered fragile. A, B. Sensitivity ranking of network species in AD versus CR cells in the absence (presence) of DHT. C. Sensitivity ranking of network species in AD cells in the absence and presence of DHT. D. Sensitivity ranking of network species in CR cells in the presence and absence of enzalutamide with a DHT stimulus.

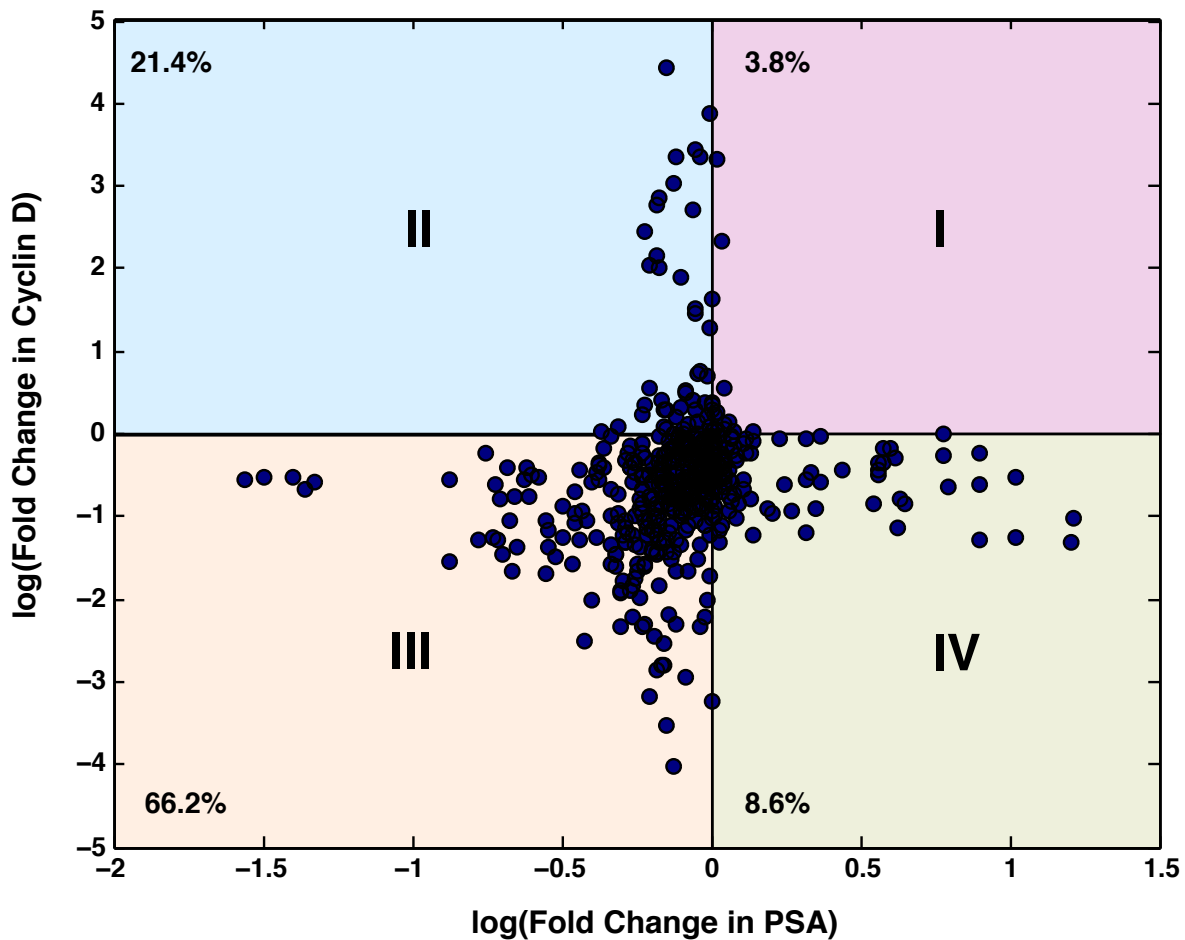


Fig. 6: Robustness analysis of a population of CR prostate models with Raf knock-out ($N = 500$). A log fold change of greater than zero implies that the concentration of the protein increased with the knock-out of Raf, while a log fold change of less than zero indicates that the concentration of protein decreased. A log of fold change equal to 0, shows no response due to Raf knock-out. Three distinct regions emerge in Raf knock-out case: (1) PSA increases, (2) cyclin D concentration increases, and (3) PSA and cyclin D concentration decrease.

917 **Supplementary materials**

918 **Estimation of a population of models using Pareto Optimal Ensemble Techniques**

919 **(POETs).** We used multiobjective optimization to estimate an ensemble of prostate mod-
920 els. Although computationally more complex than single-objective formulations, multiob-
921 jective optimization can be used to address qualitative conflicts in training data arising
922 from experimental error or cell-line artifacts [32]. In this study we used the Pareto Optimal
923 Ensemble Technique (POETs) to perform the optimization. POETs integrates standard
924 search strategies, e.g., Simulated Annealing (SA) or Local Pattern Search (PS) with a
925 Pareto-rank fitness assignment [83]. The mean squared error, η , of parameter set k for
926 training objective j was defined as:

$$\eta_j(\mathbf{p}_k) = \frac{1}{N} \sum_i^N \frac{(\hat{x}_{i,j} - \beta_j x(\mathbf{p}_k)_{i,j})^2}{\hat{\sigma}_{i,j}^2} \quad (\text{S1})$$

927 The symbol $\hat{x}_{i,j}$ denotes scaled experimental observations (from training objective j) while
928 $x(\mathbf{p}_k)_{i,j}$ denotes the simulation output (from training objective j). The quantity i denotes
929 the sampled time-index or condition, and N denotes the number of time points or condi-
930 tions for experiment j . The standard deviation, $\hat{\sigma}_{i,j}$, was assumed to be equal to 10% of the
931 reported observation, if no experimental error was reported. β_j is a scaling factor which
932 is required when considering experimental data that is accurate only to a multiplicative
933 constant. In this study, the experimental data used for training and validation was typi-
934 cally band intensity from immunoblots, where intensity was estimated using the ImageJ
935 software package [1]. The scaling factor used was chosen to minimize the normalized
936 squared error [5]:

$$\beta_j = \frac{\sum_i (\hat{x}_{i,j} x_{i,j} / \hat{\sigma}_{i,j}^2)}{\sum_i (x_{i,j} / \hat{\sigma}_{i,j})^2} \quad (\text{S2})$$

937 By using the scaling factor, the concentration units on simulation results were arbitrary,
 938 which was consistent with the arbitrary units on the experimental training data. All simu-
 939 lation data was scaled by the corresponding β_j .

940 We computed the Pareto rank of parameter set \mathbf{k}_{i+1} by comparing the simulation error
 941 at iteration $i + 1$ against the simulation archive, denoted as \mathbf{K}_i . We used the Fonseca and
 942 Fleming ranking scheme [22] to estimate the rank of the parameter set \mathbf{k}_{i+1} . Parameter
 943 sets with increasing rank are progressively further away from the optimal trade-off surface.
 944 The parameter set \mathbf{k}_{i+1} was accepted or rejected by the SA with probability $\mathcal{P}(\mathbf{k}_{i+1})$:

$$\mathcal{P}(\mathbf{k}_{i+1}) \equiv \exp \{-\text{rank}(\mathbf{k}_{i+1} | \mathbf{K}_i) / T\} \quad (\text{S3})$$

945 where T is the computational annealing temperature. The Pareto rank for \mathbf{k}_{i+1} is denoted
 946 by $\text{rank}(\mathbf{k}_{i+1} | \mathbf{K}_i)$. The annealing temperature was adjusted according to the schedule
 947 $T_k = \beta^k T_0$ where β was defined as $\beta = \left(\frac{T_f}{T_o}\right)^{1/10}$. The initial temperature was given by
 948 $T_0 = n/\log(2)$, with $n = 4$ and the final temperature $T_f = 0.1$ used in this study. The
 949 epoch-counter k was incremented after the addition of 50 members to the ensemble. As
 950 the ensemble grew, the likelihood of accepting a high rank set decreased. Parameter sets
 951 were generated by applying a random perturbation in log space:

$$\log \mathbf{k}_{i+1} = \log \mathbf{k}_i + \mathcal{N}(0, \nu) \quad (\text{S4})$$

952 where $\mathcal{N}(0, \nu)$ is a normally distributed random number with zero mean and variance ν ,
 953 set as 0.1 in this model. The perturbation was applied in log space to account for large
 954 variation in parameter scales and to ensure positive parameter values. We used a local
 955 pattern search every q steps, in our case 20, to minimize error for a single randomly se-
 956 lected objective. The local pattern-search algorithm used has been described previously
 957 [23].

958 **Table T1:** Objective function list along with species measured, stimulus, cell-type, steady state (SS) vs dynamic (D) and the corresponding literature reference.

O#	Species	Cell Type	Stimulus	SS or D	Source
959	O1	PSA	C33/C81	0	SS [48]
	O2	PSA	C33	DHT	D [48]
	O3	PSA	C81	DHT	D [48]
	O4	ERK-p	C33	DHT	D [48]
	O5	ERK-p	C81	DHT	D [48]
	O6	PSA	C33	HER2 Knockdown	SS [48]
	O7	PSA	C81	HER2 Knockdown	SS [48]
	O8	PSA	C33	MEK Up	SS [48]
	O9	PSA	C81	MEK Down	SS [48]
	O10	PSA	C33	HER2 Up	SS [48]
	O11	ERK-p	C33	HER2 Up	SS [48]
	O12	AR	C33/C51/C81	0	SS [53]
	O13	PAcP mRNA	C33	DHT	D [53]
	O14	PAcP mRNA	C51	DHT	D [53]
	O15	PAcP mRNA	C81	DHT	D [53]
	O16	HER2-p	C33/C51/C81	0	SS [103]
	O17	Cyclin D	C33/C81	0	SS CITE
	O18	Cyclin D	C33	EGF	D [68]
	O19	Cyclin D mRNA	C33	EGF	D [68]
	O20	AKT-p	C51/LNCaP-Rf	0	SS [64]
	O21	p27Kip1	C51/LNCaP-Rf	0	SS [64]
	O22	p21Cip1	C51/LNCaP-Rf	0	SS [64]
	O23	Rb-p	C33	DHT	D [99]
	O24	p70-p	C33	DHT	D [99]
	O25	p21Cip1	C33	DHT	D [45]
	O26	p27Kip1	C33	DHT	D [45]
	O27	PSA mRNA	C33	Cyclin E Up + DHT	D [100]
	O28	AR mRNA	C33	Cyclin E Up + DHT	D [100]
	O29	PSA mRNA	C33	HER2 Up	SS [101]
	O30	AKT-p	C33/C51	0	SS [51]
	O31	AR	C51	DHT	D [51]

960

O32	AR	C33	DHT	D	[11]
O33	Cyclin D1b mRNA	C33	Sam68 Knockdown	SS	[67]
O34	AR mRNA	C33	E2F Up	SS	[17]
O35	AR	C33	E2F Up	SS	[17]
O36	AR Cyclin E	C33	E2F Up	SS	[17]
O37	PSA	C33	E2F Up	SS	[17]
O38	cPAcP	C33	DHT	D	[61]
O39	Cyclin D	C33	DHT	D	[99]
O40	4EBP1-p	C33	DHT	D	[99]
O41*	PAcP mRNA	C33/C51/C81	0	SS	[53]
O42*	p16INK4	C51/C81	0	SS	[64]
O43*	cPAcP	C33/C51/C81	0	SS	[54]

Table T2: Blind Prediction list along with species measured, stimulus, cell-type, steady state (SS) vs dynamic (D) and the corresponding literature reference.

Prediction#	Species	Cell Type	Stimulus	SS or D	Source	
P1	HER2-p	C33	DHT	D	[61]	
P2	p27Kip1	C33	SHP Knockdown	D	[73]	
P3	ERK-p	C33	PAcP Knockdown	SS	[13]	
P4	AKT-p	C33	PAcP Knockdown	SS	[13]	
P5	Cyclin D1	C33	PAcP Knockdown	SS	[13]	
P6	EGFR-p	C33	EGF	D	[10]	
P7	HER2-p	C33	EGF	D	[10]	
P8	EGFR-p	LNCaP-AI	EGF	D	[10]	
P9	HER2-p	LNCaP-AI	EGF	D	[10]	
P10	CyclinE	C33	DHT	D	[45]	
P11	CDK2	C33	DHT	D	[45]	
P12	HER2-p	C33/C81	0	SS	[13]	
P13	AR	C33	EGF	D	[8]	
P14	AR	C33	EGF	D	[14]	
962	P15	p27Kip1	C33	DHT	D	[20]
P16	Rb-p	C33	DHT	D	[45]	
P17	AR	C33	DHT	D	[8]	
P18	AKT-p	C33	DHT	D	[8]	
P19	PSA	C33	EGF + DHT	D	[8]	
P20	PSA	C33	EGF	D	[8]	
P21	Cyclin D1	C33	Sam68 Knockdown	SS	[7]	
P22	Shc	C33	DHT	D	[91]	
P23	Shc	C33	EGF	D	[91]	
P24	Shc	C33/C81	0	SS	[91]	
P25	AR	C33	AKT-p Knockdown	SS	[30]	
P26	AR	LNCaP AI	AKT-p Knockdown	SS	[30]	
P27	4EBP1 bound eIF4E	C33/LNAI	0	SS	[25]	
P28	Shc-p	C33/C51/C81	0	SS	[47]	
P29	Shc-p	C33	EGF	D	[47]	
P30	PSA Response	CRPC Patients	enzalutamide	D	[76]	
P31	PSA Response	CRPC Patients	sorafenib	D	[16]	

963

P32	PSA Response	CRPC Patients	lapatinib	D	[97]
P33	PSA Response	ADPC Patients	lapatinib	D	[56]

Fig. S1: Sensitivity analysis of a population of prostate models ($N = 500$). Species with a low sensitivity are considered robust, while species with a high sensitivity ranking are considered fragile. A. Sensitivity ranking of network species in CR cells in the absence and presence of DHT. B. Sensitivity ranking of network species in CR cells in the presence and absence of enzalutamide in the absence of a DHT stimulus. C., D. Sensitivity ranking of network species in CR cells in the presence and absence of sorafenib and lapatinib, respectively, with a DHT stimulus.

Fig. S2: Robustness analysis of protein markers. Expression level of key proteins was altered by a factor of 2, 0.1, or 0 (knock-in, knock-down, or knock-out) and robustness coefficients were calculated for five key protein markers. Simulations shown were from CR cells, with indicated perturbation. Mean of 500 ensemble members is shown.